RMetS
Royal Meteorological Society

Representation of transport and scavenging of trace particles in the Emanuel moist convection scheme

Romain Pilon,[a,b]* Jean-Yves Grandpeix[a] and Philippe Heinrich[b]
[a]*Laboratoire de Météorologie Dynamique, Paris, France*
[b]*Commissariat à l'Énergie Atomique DAM-Ile de France, Arpajon Cedex, France*

*Correspondence to: R. Pilon, Laboratoire de Météorologie Dynamique, Boîte Postale 99, 4 Place Jussieu, 75252 Paris Cedex 5, France.
E-mail: romain.pilon@lmd.jussieu.fr

In the Tropics, cumulus convection has a major influence on precipitation and vertical transport of atmospheric particles, which are subject to scavenging by precipitation. A new parametrization of transport and scavenging of trace particles by convective clouds and precipitation has been developed and introduced in the Laboratoire de Météorologie Dynamique general circulation model (LMDz). This model uses the deep convection scheme of Emanuel, which is particularly suited for the Tropics. Our parametrization of transport and scavenging is closely linked to this scheme and our developments follow step-by-step the building of this convection representation. The purpose of this study is to understand better the influence of convection on the tracer vertical distribution and to assess the role of the convection parametrization.

Short-term and long-term simulations have been performed focusing on the concentrations of the natural radionuclide ^{7}Be, which is produced mainly in the stratosphere and upper troposphere and attaches to available aerosols. Single-column simulations forced by data from the Tropical Ocean–Global Atmosphere–Coupled Ocean–Atmosphere Response Experiment (TOGA–COARE) show the high efficiency of in-cloud scavenging by convective and large-scale processes in the removal of the tracer. These simulations show that, in the LMDz model, convection does not affect radionuclide concentrations as much as stratiform clouds and associated precipitation. In the free troposphere and in the boundary layer, below-cloud evaporation of rain has a major effect on tracer distribution, unlike impaction, which has a negligible effect. Three-dimensional model simulation results are compared with surface data of a station belonging to the worldwide network of the Comprehensive Nuclear Test Ban Treaty Organization (CTBTO). We show that this new parametrization is able to reproduce the observed yearly averaged concentrations of ^{7}Be at the surface and decrease by a third the overestimation of radionuclides formerly simulated without convective scavenging. LMDz simulations have been also performed over the year 2007 on a global scale using the terragenic ^{210}Pb and cosmogenic ^{7}Be radionuclides.

Key Words: parametrization; deep convection; scavenging; transport; radionuclide; climate model

Received 13 March 2013; Revised 7 July 2014; Accepted 14 July 2014; Published online in Wiley Online Library 16 September 2014

1. Introduction

In the Tropics, deep convection has a substantial influence on large-scale circulation and on water distribution in the troposphere. Moreover, it greatly impacts aerosol vertical distribution, which is controlled not only by air transport but also by scavenging, the cleansing of material from the atmosphere by hydrometeors. In the last two decades, the complexity and realism of the representation of this process in climate models has been increasing. However, representations of scavenging differ from one general circulation model (GCM) to another. As reported in Rasch *et al.* (2000), results from model intercomparison underline uncertainties that come from either transport and scavenging parametrizations or deep convective cloud parametrization (see Mahowald *et al.*, 1995; Tost *et al.*, 2006, 2010). Nevertheless, Koch *et al.* (1996), Liu *et al.* (2001) and Heinrich and Jamelot (2011) note that the surface concentration of ^{7}Be in the Tropics is generally overestimated, owing to insufficient scavenging within convective clouds or removal by precipitation. So far, the parametrization of wet removal by convective clouds and precipitation distinguishes in-cloud scavenging, below-cloud impaction and release by evaporation.

Representation of scavenging processes is generally based on prescribed in-cloud scavenging ratios and implicitly parametrizes nucleation and impaction processes using the formulation of Giorgi and Chameides (1986). Some authors separate in-cloud scavenging from scavenging in convective updraughts (Lawrence and Rasch, 2005). Some calculate below-cloud impaction and release by evaporation using constant rates or depending on precipitation and evaporation rates (Liu *et al.*, 2001; Reddy and Boucher, 2004), while others use a complex formulation of microphysics in an effort to gain accuracy (Andreae and Rosenfeld, 2008; Croft *et al.*, 2010).

Here, our approach is to develop a parametrization based on the moist convective scheme of Emanuel (1991). The main asset of this scheme is the precipitating downdraughts, which are greatly involved in deep convective processes. It is a feature expected to play a key role for tracers originating in the upper troposphere, such as ^{7}Be. The parametrization is expected to provide feedback on the moist convective scheme parameters, such as the fractional area covered by these precipitating downdraughts. The new parametrization closely follows the physical mechanisms of the Emanuel scheme, the processes in up- and downdraughts of deep convection and exchanges between them at each level.

The model used for this study is the Laboratoire de Météorologie Dynamique GCM (LMDZ: Hourdin *et al.*, 2006), more specifically its version used for the third Coupled Model Intercomparison Project (CMIP3) simulations. In this model, moist processes are represented by two parametrizations: deep convection (Emanuel, 1991) and large-scale condensation processes (Le Treut and Li, 1991). Our approach is to deal separately with the tracer transport and scavenging associated with these two schemes: (i) for large-scale condensation, we keep a standard description comprising three parts – in-cloud scavenging, below-cloud scavenging and release by rain evaporation; the corresponding schemes are briefly described in the Appendix; and (ii) for deep convection, we designed a new parametrization, which accounts for transport as well as scavenging in the various vertical draughts.

An overview of the existing scavenging parametrizations in the LMDz climate model is provided in Heinrich and Jamelot (2011). The simulations use the natural radionuclide ^{7}Be as a passive tracer for assessing our parametrization. Associated with the ^{210}Pb radionuclide, ^{7}Be has been widely used to evaluate atmospheric transport and aerosol removal processes in GCMs (Balkanski *et al.*, 1993; Koch *et al.*, 1996; Liu *et al.*, 2001). Thanks to the low (high) altitude of the tropospheric source of ^{210}Pb (^{7}Be), the combined study of these tracers is particularly interesting in the Tropics in order to analyze the role of scavenging by large-scale and convective processes.

The aim of this research is to diagnose how the processes in deep convection influence the vertical tracer distribution and its elimination by precipitation.

The present article is devoted to the presentation of this new scavenging parametrization, coupled with the Emanuel convective scheme. The formulation of the transport and scavenging model is presented in section 2. Section 3 evaluates the scheme in a single-column model simulation (SCM). In section 4, the parametrization is tested in the GCM LMDz at a global scale and results are compared with observations at a tropical station. Lastly, we summarize and discuss the features of this new scavenging scheme.

2. Model description

The new parametrization of transport and scavenging describes the redistribution and removal of tracers in deep convective clouds by rain inside and below the clouds. It is tested in the LMDz general circulation model. It is implemented within the Emanuel convection scheme (see Emanuel, 1991; Emanuel and Živković-Rothman, 1999).

The presentation of our scheme follows the one of Emanuel (1991) and we use the same notations for mass fluxes. The only difference is that all fluxes are defined as a function of continuous vertical levels z instead of discrete layers. The parametrization of transport and scavenging is separated into two parts: transport and scavenging in the saturated updraughts and downdraughts and transport and scavenging in the unsaturated downdraughts. (We shall not use the usual terms 'in-cloud' and 'below-cloud' scavenging, since, in the Emanuel parametrization, a fraction of the precipitation falls through the cloud). In the study, the moist convective scheme does not include ice thermodynamics, which could affect the role of convective precipitation in the upper troposphere. However, as noted by Liu *et al.* (2001), observations (Jacob, 2000) show that, within the convective updraughts, aerosols incorporated into the cloudy air are incorporated in the condensed phase of water irrespective of the nature of the condensed phase.

The effect of deep convective cloud on the environmental tracer distribution $\tilde{C}$ is split into two tendencies, $\left(\partial_t \tilde{C}\right)_{\text{sat}}$ and $\left(\partial_t \tilde{C}\right)_{\text{unsat}}$, induced by saturated draughts and unsaturated draughts on the environment, respectively:

$$\left(\partial_t \tilde{C}\right)_{\text{cv}} = \left(\partial_t \tilde{C}\right)_{\text{sat}} + \left(\partial_t \tilde{C}\right)_{\text{unsat}}, \tag{1}$$

where $\tilde{C}$ is the tracer number concentration in the environment. In each tendency, the mass balancing displacement is included as in the Emanuel scheme. This splitting allows a separation of the processes, i.e. the amount of tracers coming from $\left(\partial_t \tilde{C}\right)_{\text{sat}}$ comes from the saturated processes and that coming from $\left(\partial_t \tilde{C}\right)_{\text{unsat}}$ comes from the evaporation of precipitation and from the detrainment of the precipitating downdraught into the environment. The parametrizations of each tendency are detailed in sections 2.4 and 2.5.

2.1. *Short description of Emanuel scheme*

The representation of convection follows the scheme of Emanuel (1991) and is based on the idea that convective clouds are not homogeneous in nature: the cloud is represented by multiple vertical draughts moving adiabatically between levels where mixing with environmental air occurs.

Air below the cloud base ascends adiabatically, forming updraughts, and lifts unmixed up to some level z', between the cloud base and the level of neutral buoyancy. At each level z', a fraction $\epsilon(z')$ of condensed water (l_a) produced during the ascent is converted into precipitation and is defined by Emanuel (1991) such that $\epsilon(z)$ varies linearly from 0 to $\epsilon_{\max}$ between 150 and 500 hPa above the lifting condensation level (LCL) and is constant elsewhere.

The maximum precipitation efficiency is a little lower than unity (0.999) to allow cloud water to remain in suspension in the upper troposphere (Bony and Emanuel, 2001). The air from the adiabatic updraught, the liquid water content of which is now $(l_a[1 - \epsilon(z')])$, is mixed at level z' with environmental air, yielding a spectrum of mixtures. Each mixture moves adiabatically up or down to its level z (z can be higher or lower than z') of neutral buoyancy – in ascending mixtures, water may condense and precipitate – and then, after removal of precipitation, detrains in the environment.

Precipitation formed in adiabatic ascents and in the mixtures is added to a single precipitating downdraught driven by the evaporation of the rain.

Deep convective clouds cover an area smaller than the grid cell S_t. When precipitation occurs, it forms a precipitating downdraught covering a region S_d. The fractional area covered by the unsaturated downdraught $\sigma_d = S_d/S_t$ is prescribed by Emanuel: the draught covers only 1% of the grid cell, a small region compared with large-scale clouds and precipitation, which may cover a major fraction of the grid cell. In this type of spatial coverage, aerosols would be less subject to removal by convective precipitation than by large-scale precipitation.

2.2. Assumptions on aerosols

The LMDz climate model does not yet distinguish the different aerosol modes. The tracers used this study are radionuclides ^{210}Pb and ^{7}Be, which attach themselves to all available submicrometric hydrophilic aerosols of the accumulation mode (Bondietti *et al.*, 1987). In addition, ^{210}Pb also attaches itself to hydrophobic aerosols according to its concentration. From that perspective, we treat ^{210}Pb like ^{7}Be and a monodisperse distribution size is considered. Furthermore, in the model all aerosol particles act as condensation nuclei irrespective of the temperature. According to the sizes of the aerosols that bear these two radionuclides (Bondietti *et al.*, 1987; Winkler *et al.*, 1998; Marley *et al.*, 2000), they belong to the Greenfield gap and are thus in accumulation mode; as we use a monodisperse distribution for aerosols, Brownian motion and inertial impaction processes can be neglected (Greenfield, 1957). For simplicity, we did not parametrize these processes.

2.3. Notations and conventions

In order to simplify the writing of following equations, we use a specific notation. Let us use C_x^y to denote the amount of tracer per unit of mass of phase x ('c' for cloudy condensate, 'p' for precipitating water and 'v' for air/vapour mixture) in draught y ('a' for adiabatic ascent, 'm' for mixed draughts, 'd' for the saturated downdraught, 'u' for the saturated updraught and 'p' for a precipitating downdraught). In the case of radionuclides, the amount of tracer is measured by its activity (as is usual in the literature). The quantity C_x^y is hereafter called the tracer concentration.

We use M to represent mass fluxes: M_a for the adiabatic updraught, $\tilde{M}$ for the environment, M_p for the precipitating downdraught; $(\partial^2 M_\mathrm{a}/\partial z)\,\delta z$ is the mass flux of the adiabatic draught ending in the layer $[z, z+\delta z]$. $(\partial M_\mathrm{m}/\partial z \partial z')\,\delta z\,\delta z'$ is the mass flux of the mixed draught going from layer $[z', z'+\delta z']$ to $[z, z+\delta z]$. All mass fluxes are defined positive upward.

Variables related to draughts going from z' to z are indexed zz', e.g. $F^{zz'}$ is the fraction of environment air entrained at z' in the draught going to z. z_b is the altitude of the cloud base and z_t that of the cloud top. More generally, all variables with a tilde refer to the environment.

2.4. Saturated updraughts and downdraughts

In this section, we describe the transport and scavenging of tracers in the saturated draughts of a deep convective cloud.

The tendency of tracer concentration induced by a saturated draught in the environment is the sum of the effects of entrainment, detrainment and convergence of the subsiding mass flux $\tilde{M}\tilde{C}$:

$$\rho\,\left(\partial_\mathrm{t}\tilde{C}\right)_\mathrm{sat} = d_C - e_{\tilde{C}} - \frac{\partial(\tilde{M}\tilde{C})}{\partial z}\,, \tag{2a}$$

where d_C and $e_{\tilde{C}}$ are the fluxes of tracers in the detrainment and entrainment, respectively, and ρ is the density of air. Using the environment mass-budget equation $\partial_z\tilde{M} = d - e$, where d and e are the detrained and entrained mass fluxes, and assuming that the tracer concentration in entrained air is equal to $\tilde{C}$, one may simplify Eq. (2a) into

$$\rho\,\left(\partial_\mathrm{t}\tilde{C}\right)_\mathrm{sat} = d_C - d\,\tilde{C} - \tilde{M}\,\frac{\partial\tilde{C}}{\partial z}\,, \tag{2b}$$

where the mass flux of detrained tracers d_C still needs to be defined. To calculate the tendency d_C, the contribution of each draught is calculated separately, considering the condensed phase and the vapour phase.

We assume thereafter that the fraction of tracers included in the vapour phase is constant along adiabatic displacements, i.e. after initiation of condensation no further activation occurs.

2.4.1. Adiabatic ascent

Adiabatic ascent is fed by tracers in the layer going from the surface to an altitude h_s ($h_\mathrm{s} = 100$ m) below z_b, the cloud base. The tracer concentration within this flux is given by

$$C^\mathrm{a} = \frac{1}{h_\mathrm{s}}\int_0^{h_\mathrm{s}} \tilde{C}(z)\,\mathrm{d}z\,. \tag{3}$$

Air and tracers are lifted unmixed from the cloud base to an arbitrary level z' between the cloud base and the level of neutral buoyancy. During the ascent, a fraction α_a of tracers serving as cloud condensation nuclei (CCN) is supposed to be activated into droplets and incorporated within cloud water. $(1-\alpha_\mathrm{a})$ stays in vapour. At z', when the adiabatic updraught stops, a fraction $\epsilon(z')$ of cloud water precipitates, which removes $\epsilon(z')\,\alpha_\mathrm{a}$ of the tracers.

2.4.2. Mixture

The remaining cloudy air, with tracer concentration $C^\mathrm{a}\big(1-\epsilon(z')\,\alpha_\mathrm{a}\big)$, is mixed at level z' with environmental air before being displaced to z. Upon mixing with adiabatic ascent air, a fraction β_m of the CCN present in the entrained air is activated, while $(1-\beta_\mathrm{m})$ stays in the vapour phase. As regards air coming from the adiabatic ascent, we assume that tracers that belonged to the condensed and gaseous phases before mixing also belong to the condensed and gaseous phases, respectively, after mixing.

The amount of tracer in the condensed phase of a mixture of mass δm_m formed at level z', going to level z and made of a fraction $F^{zz'}$ of environment air and $(1-F^{zz'})$ of adiabatic ascent air, is therefore $\delta m_\mathrm{m}\left(\big[1-\epsilon(z')\big]\,\alpha_\mathrm{a}\,C^\mathrm{a}\,(1-F^{zz'}) + \beta_\mathrm{m}\,\tilde{C}(z')\,F^{zz'}\right)$. Since the amount of tracer present in the condensed phase is constant under adiabatic displacement, this is also equal to the amount of tracer present in the condensed phase when the mixture reaches level z: $\delta m_\mathrm{m}\,C_\mathrm{c}^\mathrm{m}(z,z')\,l_\mathrm{m}^{zz'}$. Hence, the concentration of tracer in the condensed phase at level z reads

$$\begin{aligned} C_\mathrm{c}^\mathrm{m}(z,z') = \Big(&\big[1-\epsilon(z')\big]\,\alpha_\mathrm{a}\,C^\mathrm{a}\big(1-F^{zz'}\big) \\ &+ \beta_\mathrm{m}\,\tilde{C}(z')\,F^{zz'}\Big) / l_\mathrm{m}^{zz'}\,. \end{aligned} \tag{4a}$$

Likewise, the concentration in the vapour phase reads

$$\begin{aligned} C_\mathrm{v}^\mathrm{m}(z,z') = \Big[&(1-\alpha_\mathrm{a})\;C^\mathrm{a}\left(1-F^{zz'}\right) \\ &+ (1-\beta_\mathrm{m})\;\tilde{C}(z')\,F^{zz'}\Big] / \left(1-l_\mathrm{m}^{zz'}\right)\,. \end{aligned} \tag{4b}$$

According to their buoyancy, mixtures either descend or ascend to a level z. Descending mixtures (saturated downdraught) are detrained without further precipitation formation. The amount of detrained tracer is then the sum of the amount of tracer in the two water phases. The tracer concentration in the saturated downdraught is

$$\begin{aligned} C^\mathrm{d}(z,z') = &\;\tilde{C}(z')\,F^{zz'} \\ &+ \left(1-F^{zz'}\right)\left(C^\mathrm{a} - \epsilon(z')\,\alpha_\mathrm{a}\,C^\mathrm{a}\right)\,. \end{aligned} \tag{5a}$$

If mixtures ascend, additional condensation is produced ($l_\mathrm{m}^{zz'}$) and might precipitate. A fraction ϵ_m of condensed water is converted into precipitation at z in these mixtures. Then $(1-\epsilon_\mathrm{m})$ is the fraction of water detrained to z without precipitating. After precipitation formation, there remains C^u in the saturated updraught:

$$\begin{aligned} C^\mathrm{u}(z,z') = &\;C_\mathrm{v}^\mathrm{m}(z,z')\left(1-l_\mathrm{m}^{zz'}\right) \\ &+ \left(1-\epsilon_\mathrm{m}^{zz'}\right)\;C_\mathrm{c}^\mathrm{m}(z,z')\,l_\mathrm{m}^{zz'}\,, \end{aligned} \tag{5b}$$

and $\epsilon_{\rm m}$ is given by

$$\epsilon_{\rm m}^{zz'} = \sup\Big(0,\ 1 - \big[1 - \epsilon(z)\big]\, l_{\rm a}(z)\Big) \,/\, l_{\rm m}^{zz'}\,, \tag{6}$$

where $[1 - \epsilon(z)]\, l_{\rm a}(z)$ is the remaining condensate in the adiabatic ascent at z after precipitation removal.

2.4.3. *Precipitation*

Tracers in water converted into precipitation at the end of the adiabatic ascent and within the mixtures are further injected into the precipitation of the unsaturated downdraught (see section 2.4). The tracer concentrations in the precipitation do not play any role in the determination of $(\partial_{\rm t}\tilde{C})_{\rm sat}$, but will be important later for the determination of $(\partial_{\rm t}\tilde{C})_{\rm unsat}$ (section 2.5).

Using $l_{\rm a}$, $l_{\rm m}^{zz'}$, $\epsilon(z)$ and $\epsilon_{\rm m}^{zz'}$ makes it possible to determine tracer concentration in the precipitation associated with the adiabatic ascent or with the mixtures. The concentration of tracer into the precipitation coming from the adiabatic ascent, $C_{\rm p}^{\rm a}$, may be written as

$$C_{\rm p}^{\rm a}(z) = \frac{\alpha_{\rm a}\, C^{\rm a}}{l_{\rm a}(z)}\,. \tag{7}$$

The concentration, $C_{\rm p}^{\rm m}(z)$, in the condensed water converted into precipitation (mixed at z' and displaced to z) within all mixed draughts arriving in z may be written as

$$C_{\rm p}^{\rm m}(z) = \frac{\displaystyle\int_{z_{\rm b}}^{z} C_{\rm c}^{\rm m}(z,z')\,\epsilon_{\rm m}^{zz'}\, l_{\rm m}^{zz'}\,\frac{\partial^2 M_{\rm m}}{\partial z\,\partial z'}\,{\rm d}z'\,{\rm d}z}{\displaystyle\int_{z_{\rm b}}^{z} \epsilon_{\rm m}^{zz'}\, l_{\rm m}^{zz'}\,\frac{\partial^2 M_{\rm m}}{\partial z\,\partial z'}\,{\rm d}z'\,{\rm d}z}\,. \tag{8}$$

2.4.4. *Final formulation*

The flux of tracer detrained at level z takes account of both concentrations $C^{\rm d}$ (Eq. (5a)) and $C^{\rm u}$ (Eq. (5b)) and is given by

$$\begin{aligned} d_C(z)\,{\rm d}z = &\int_{z_{\rm b}}^{z} \frac{\partial^2 M_{\rm m}}{\partial z\,\partial z'}\; C^{\rm u}(z',z)\,{\rm d}z'\,{\rm d}z \\ &+ \int_{z}^{z_{\rm t}} \frac{\partial^2 M_{\rm m}}{\partial z\,\partial z'}\; C^{\rm d}(z',z)\,{\rm d}z'\,{\rm d}z\,. \end{aligned} \tag{9a}$$

The detrained mass flux reads

$$d(z)\,{\rm d}z = \int_{z_{\rm b}}^{z_{\rm t}} \frac{\partial^2 M_{\rm m}}{\partial z\,\partial z'}\;{\rm d}z'\,{\rm d}z\,. \tag{9b}$$

Using Eqs (9a) and (9b) with Eq. (2b), with some algebra, the tendency induced by the saturated draught is

$$\begin{aligned} \rho\,\big(\partial_{\rm t}\tilde{C}\big)_{\rm sat} = &\big(C^{\rm a} - \tilde{C}(z)\big)\int_{z_{\rm b}}^{z_{\rm t}} \frac{\partial^2 M_{\rm m}}{\partial z\,\partial z'}\big(1 - F^{zz'}\big)\,{\rm d}z' \\ &+ \int_{z_{\rm b}}^{z_{\rm t}} \frac{\partial^2 M_{\rm m}}{\partial z\,\partial z'}\,F^{zz'}\,\big(\tilde{C}(z') - \tilde{C}(z)\big)\,{\rm d}z' \\ &- \tilde{M}\,\frac{\partial \tilde{C}}{\partial z} + \rho\,\big(\partial_{\rm t}\tilde{C}\big)_{\rm scav}\,, \end{aligned} \tag{10a}$$

where the first term corresponds to tracers in the mass flux supplied by the adiabatic ascent to the mixtures, the second one to tracers in the mass flux taken from the environment to the mixtures, $\tilde{M}\,\dfrac{\partial \tilde{C}}{\partial z}$ is the compensating subsidence and the last term is the tendency induced by the scavenging, which is

$$\begin{aligned} \rho\,\big(\partial_{\rm t}\tilde{C}\big)_{\rm scav} = &-\alpha_{\rm a}\,C^{\rm a}\int_{z_{\rm b}}^{z_{\rm t}} \frac{\partial^2 M_{\rm m}}{\partial z\,\partial z'}\big(1 - F^{zz'}\big)\,\epsilon(z')\,{\rm d}z' \\ &- \alpha_{\rm a}\,C^{\rm a}\int_{z_{\rm b}}^{z} \frac{\partial^2 M_{\rm m}}{\partial z\,\partial z'}\big(1 - F^{zz'}\big)\epsilon_{\rm m}^{zz'}\big[1 - \epsilon(z')\big]\,{\rm d}z' \\ &- \beta_{\rm m}\int_{z_{\rm b}}^{z_{\rm t}} \frac{\partial^2 M_{\rm m}}{\partial z\,\partial z'}\,F^{zz'}\;\epsilon_{\rm m}^{zz'}\,\tilde{C}(z')\,{\rm d}z'\,. \end{aligned} \tag{10b}$$

The first term corresponds to tracers removed by precipitation formation in the adiabatic ascent, the second one to tracers originating from the adiabatic ascent removed inside the mixtures and the last one to tracers of the environment removed by precipitation formation inside the mixtures.

If deep convective scavenging is disabled, $\big(\partial_{\rm t}\tilde{C}\big)_{\rm scav} = 0$. Tracers are only transported by air flow without being transformed into CCN.

2.5. *Unsaturated downdraughts*

Following Emanuel, the unsaturated downdraught is separated into two parts: the precipitating water on one hand and the air flowing down in the draught on the other hand, the latter being partly cloudy and partly clear. Falling precipitation evaporates into the clear air. For simplicity, the air flowing down in the draught is called unsaturated air.

Within a layer at level z with thickness δz, as depicted in Figure 1, precipitation flux P (precipitation per unit area of the model grid) is fed by precipitation formed from water condensed within the adiabatic ascent $(\partial P_{\rm a}/\partial z)\delta z$ and within mixed draughts $(\partial P_{\rm m}/\partial z)\delta z$. The two sources of precipitation $(\partial P_{\rm a}/\partial z)\delta z$ and $(\partial P_{\rm m}/\partial z)\delta z$ can be expressed in terms of the mass fluxes of the updraughts reaching that layer ($(\partial M_{\rm a}/\partial z)\delta z$ for the adiabatic ascent and $\int_{z_{\rm b}}^{z}(\partial^2 M_{\rm m}/\partial z\partial z')\,{\rm d}z'\;\delta z$ for the mixed updraughts), their condensed water contents $l_{\rm a}$ and $l_{\rm m}^{zz'}$ and the rates of conversion into precipitation $\epsilon(z')$ and $\epsilon_{\rm m}^{zz'}\,l_{\rm m}^{zz'}$:

$$\frac{\partial P_{\rm a}}{\partial z}\delta z = \frac{\partial M_{\rm a}}{\partial z}\delta z\;\epsilon(z)\,l_{\rm a}(z)\,, \tag{11a}$$

and

$$\frac{\partial P_{\rm m}}{\partial z}\delta z = \int_{z_{\rm b}}^{z} \frac{\partial^2 M_{\rm m}}{\partial z\,\partial z'}\,\epsilon_{\rm m}^{zz'}\,l_{\rm m}^{zz'}\;{\rm d}z'\;\delta z\,. \tag{11b}$$

Precipitation has a major influence on the tracers distribution in the environment. Let $\delta\Psi$ be the mass of evaporated water in a given layer $[z, z+\delta z]$ per unit time within the fractional

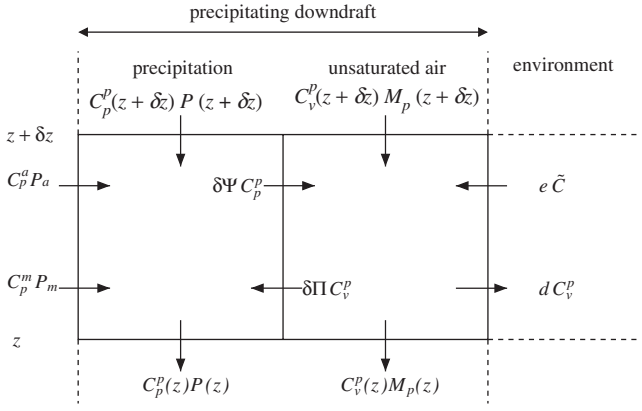

Figure 1. Sketch of an unsaturated downdraught and exchanges of tracers between precipitation, unsaturated air and environment.

area covered by the downdraughts σ_d. This mass can only evaporate within the fraction σ_s of precipitation falling in clear air: $\delta\Psi = \sigma_s\sigma_d E\,\rho\,\delta z$, where E is the evaporation rate (see eq. (12b) from Emanuel, 1991). Thus evaporation of precipitation increases by $\delta\Psi\ C_p^p$ (C_p^p is the tracer concentration in the precipitation) the tracer amount in the unsaturated air $\rho\,\delta z\,C_v^p$.

Let $\delta\Pi$ be the effective mass of the precipitating downdraught swept by the rain in the same layer per unit time within σ_d: $\delta\Pi = \sigma_d\,\Lambda\,\rho\,\delta z$, where Λ is the scavenging coefficient described hereinafter. Raindrops impact aerosols and remove $\delta\Pi\,C_v^p$ tracers from the unsaturated air. Moreover, the unsaturated downdraught exchanges tracers with the environment by entrainment and detrainment according to the entrained mass flux e and the detrained mass flux d, respectively.

We calculate a tendency in which all above-mentioned exchanges are represented, to determine the effects of the unsaturated downdraught on the environment. This tendency, $\partial_t C_{unsat}$, is given by

$$\rho\,\left(\partial_t\tilde{C}\right)_{unsat} = d\,C_v^p - e\,\tilde{C} - \frac{\partial\tilde{M}\tilde{C}}{\partial z}\,. \tag{12a}$$

Since the environmental mass flux $\tilde{M}$ is equal to the opposite of the unsaturated downdraught mass flux M_p and as $\partial_z\tilde{M} = e - d$, the tendency may be written as

$$\rho\,\left(\partial_t\tilde{C}\right)_{unsat} = d\left(C_v^p - \tilde{C}\right) + M_p\,\partial_z\tilde{C}\,, \tag{12b}$$

where $M_p\,\partial_z\tilde{C}$ denotes the transport in the compensating ascent induced by the unsaturated downdraught.

To solve Eq. (12b), the tracer concentration in unsaturated air C_v^p is required. As the unsaturated draught is a steady system for each layer $[z, z+\delta z]$, budget equations can be established to describe the evolution of the draught. It is a two-way exchange of mass between precipitation, unsaturated air and environmental clear air, as shown in Figure 1, taking into consideration the water phase change. The amount of tracer in the precipitation between z and $z+\delta z$ takes into account the variation of the flux of tracer transported by the precipitation ($-\,\partial_z\left(P\,C_p^p\right)\,\delta z$). It is enriched by those in the sources of precipitation ($+\,\partial_z P_a\,C_p^a\,\delta z$ and $+\,\partial_z P_m\,C_p^m\,\delta z$) and by tracer of the unsaturated air impacted by the precipitation ($+\,\delta\Pi\,C_v^p$); it is impoverished when tracers are released by evaporation of the precipitation ($-\,\delta\Psi\,C_p^p$). On the other side, the amount of tracer in the precipitating downdraught takes into account the variation of tracer in unsaturated air $[-\,\partial_z\left(M_p\,C_v^p\right)]$. The precipitating downdraught is driven by the evaporation of the precipitation, enriching the unsaturated air of $+\,\delta\Psi\,C_p^p$ tracers, and this process therefore controls the entrainment (enrichment) of environment tracers ($+\,e\,\delta z\,\tilde{C}$) and the detrainment (impoverishment) of tracers of the unsaturated air to the environment ($-\,d\,\delta z\,C_v^p$). Moreover, precipitation impaction reduces the concentration within the unsaturated air ($-\,\delta\Pi\,C_v^p$).

Summing up these various exchanges yields the following first-order differential equation for $C_p^p(z)$ and $C_v^p(z)$ with top boundary conditions $C_p^p(z_t) = C_v^p(z_t) = 0$:

$$\begin{cases} -\partial_z\left(P\,C_p^p\right) + \partial_z P_a\,C_p^a + \partial_z P_m\,C_p^m \\ \qquad\qquad -\mathrm{d}\Psi/\mathrm{d}z\,C_p^p + \mathrm{d}\Pi/\mathrm{d}z\,C_v^p = 0, \\ -\partial_z\left(M_p\,C_v^p\right) + e\,\tilde{C} - d\,C_v^p \\ \qquad\qquad +\mathrm{d}\Psi/\mathrm{d}z\,C_p^p - \mathrm{d}\Pi/\mathrm{d}z\,C_v^p = 0\,. \end{cases} \tag{13}$$

If scavenging is disabled, i.e. if tracers are transported only by the air flow of the unsaturated downdraught, terms related to the precipitation and evaporation are not involved in the system of equations (Eq. (13)), which becomes

$$e\,\tilde{C} - d\,C_v^p = \partial_z\left(M_p\,C_v^p\right)\,. \tag{14}$$

In this case, the environmental tracer distribution is consequently closely related to the compensating ascent rather than the precipitation.

2.5.1. *Impaction scavenging coefficient:* Λ

Usually, impaction by rain is represented by a coefficient calculated using a collision efficiency, which implicitly takes into account several microphysical processes (see Sportisse, 2007). This latter coefficient is defined for monodisperse or polydisperse raindrops as well as for a particle size distribution (see for instance Mircea *et al.*, 2000). The collision efficiency includes impaction, split into three processes that are particle size-dependent: Brownian diffusion, interception and inertial impaction (Slinn, 1983) for ultrafine, fine and coarse particles, respectively. The scavenging coefficient is proportional to the collision efficiency and raindrop and particle sizes, as well as the raindrop terminal velocity.

For simplicity, in our parametrization, as we consider only deep convection and associated rains, we neglect Brownian diffusion and inertial impaction. We assume that the impaction efficiency, $\mathcal{E}_{imp}$, is set to 10^{-3} (as a standard value for the range of the size of particles studied, i.e. (0.6–1) µm). We also assume that, following Emanuel (1991), the rain velocity is equal to its terminal velocity w_t, set to $45\,\mathrm{Pa\,s^{-1}}$. We use a monodisperse size distribution for raindrops: the raindrop diameter is set at 2 mm (value from Pruppacher and Klett (1996) for a tropical storm with heavy rainfall over Hawaii).

The temporal variation of mass of tracers removed from the unsaturated downdraught air,

$$\frac{\mathrm{d}\Pi}{\mathrm{d}z}\,C_v^p = -\rho\,\left(\partial_t C_v^p\right)_{imp},$$

is the temporal variation of the mass of tracers in the volume swept by n_d falling raindrops in the precipitating column over the surface covered by the downdraught and is given by

$$\rho\,\left(\partial_t C_v^p\right)_{imp} = -\rho\,C_v^p\,n_d\,\mathcal{E}_{imp}\,w_t\pi\,r^2\,, \tag{15}$$

where r is the radius of raindrops.

This equation can be related to the Emanuel scheme using the precipitation flux P. Indeed, the precipitation flux combined with the flux of falling raindrops may be written as

$$P = \frac{4}{3}\pi\,r^3\,n_d\,w_t\,\rho_l\,\sigma_d\,, \tag{16}$$

with ρ_l the density of liquid water. Thus, using Eq. (15) together with Eq. (16), we obtain

$$\rho\,\left(\partial_t C_v^p\right)_{imp} = -\Lambda\,\rho\,C_v^p\,, \tag{17a}$$

where the scavenging coefficient Λ is

$$\Lambda = \mathcal{E}_{imp}\,\frac{3\,P}{4\,\rho_l\,\sigma_d\,r}. \tag{17b}$$

In our model, precipitation has the same effect on tracers when falling through saturated air, unsaturated air and clear air; thus Λ is independent of the fraction of precipitation falling in clear air σ_s.

2.6. *Sum up*

The convective transport scheme is now complete: the resolution of the first-order differential equation (Eq. (13)) associated with the diagnostic variable Λ (Eq. (17b)) allows us to determine Eq. (12b); combined with Eq. (2a) (composed of Eqs (10a) and (10b)), the final solution of the tendency

of tracer concentration induced by the convection (Eq. (1)) can be solved. In-cloud scavenging is characterized by two parameters representing two microphysical properties: CCN activation in adiabatic ascent and mixtures, α_a and β_m, respectively. Impaction by rain depends on the collision efficiency parameter $\mathcal{E}_{imp}$.

The tracer sink in the saturated draught tendency (Eq. (10b)) is equal to the tracer source for the unsaturated downdraughts. The latter redistributes these tracers partly in the atmosphere, partly at the surface.

The discretization uses a staggered grid for the mass and precipitation fluxes, $\tilde{M}$, M_p and P, respectively. As the concentrations C_p^p and C_v^p are calculated on the centred grid, to solve (Eq. (13)) we use the upstream scheme.

3. 1D atmospheric simulation

3.1. Simulation of the TOGA–COARE case

For evaluation purposes, the one-dimensional version of the atmospheric model LMDz is applied to the TOGA–COARE case (Ciesielski *et al.*, 2003).

TOGA–COARE is an international campaign, which was conducted from 1 November 1992 to 28 February 1993 in the western Pacific warm pool centred at 2°S and 155°E. This region is associated with a warm sea-surface temperature (SST; during the four months the SST was 29.4 ° C on average). Within this period, two Madden–Julian oscillation (MJO) active phases occurred, during the second half of December and during February (Chen *et al.*, 1996; Yanai *et al.*, 2000). Between 20 and 24 December, maximum convection developed and this reached its peak on 24 December. These two phases are interspersed with a low convective activity period. During the experiment, the two MJO active phases in the Pacific Ocean are related to the presence of two convective clusters.

This atmospheric variability is particularly interesting to study the correlation of the tracer distribution with the convective activity. In the literature, observations of the campaign have been used to optimize Emanuel's convective scheme (Emanuel and Živković-Rothman, 1999), validate simulated isotopic compositions of water (Bony *et al.*, 2008) or model tracer transport using a cloud-resolving model (Salzmann *et al.*, 2004).

We use a single column model with physical parametrizations close to that of Hourdin *et al.* (2006), except for an extension of the model to the stratosphere (Hourdin *et al.*, 2012a,b): the vertical resolution is increased to 39 layers (the grid is stretched near the surface: first grid point at 35 m and eight grid points in the first kilometre; mean resolution of 800 m between 1 and 20 km and the last point at 40 km). As the SCM is forced by TOGA–COARE data sets throughout the four months, simulated precipitation is in close agreement with available observations, as shown for daily precipitation in Figure 2(a). Transport and convective scavenging of aerosols are parametrized in the previous section. For simplicity, we do not consider the subtlety of droplet formation processes: all CCN are assumed activated, $\alpha_a = 1$ and $\beta_m = 1$.

The removal of tracers in stratiform clouds and by large-scale precipitation is also included in the model and is based on the parametrization of Reddy and Boucher (2004, hereinafter referred to as RB04) close to the formulation of Giorgi and Chameides (1986), but with some changes such that the description of the scavenging process follows the large-scale condensation parametrization more closely. This scheme does not differentiate ice nucleation from water nucleation. More explanations of this scheme can be found in the Appendix.

Tracer vertical advection is calculated from the forced vertical velocity. Horizontal advection is supposed to bring air of the same composition as the grid-cell air (horizontal winds cannot sweep away radionuclides from the region).

3.2. Radionuclide tracer

As its source is mainly located in the upper troposphere and above, ^{7}Be is an appropriate tracer for parametrization assessment purposes and for emphasizing the role of precipitation and convective downdraughts.

^{7}Be is a natural radionuclide (half-life of 53.3 days) and a useful tracer of the short-term atmospheric processes. It has a global continuous well-known source and is naturally produced by spallation reactions induced by high-energy cosmic ray protons and neutrons on nitrogen and oxygen in the stratosphere and upper troposphere (Lal and Peters 1967, hereinafter LP67). After its production, ^{7}Be attaches indiscriminately to ambient submicrometric aerosols (Bondietti *et al.*, 1987) and is transported by them. ^{7}Be is chemically nonreactive and may be considered as a passive tracer. It is removed by radioactive decay and by wet and dry deposition, although the dominating removal process is scavenging by convective and large-scale precipitation. Thus the mean residence times in the troposphere range from 10 to 35 days (Shapiro and Forbes-Resha, 1976; Bleichrodt, 1978; Koch *et al.*, 1996; Liu *et al.*, 2001). Despite the different temporal variabilities of this radionuclide concentration, reported in LP67 and Koch and Mann (1996), interannual ^{7}Be surface concentration variability is negligible, as reported by Yoshimori (2005).

In our model, the source of the radionuclide is an adaptation of LP67 with constant concentrations depending on the latitude and the model layers but not on the solar activity. The initial tracer profile is taken from a previous GCM simulation (Heinrich and Jamelot, 2011) at 2°S and 155°E, the location of TOGA–COARE.

3.3. Results

The numerical experiments have been performed over a period of four months. We focus on two different periods, showing the alternation between active and suppressed phases of the MJO, which are characterized by high and low convective intensity, respectively.

As described by Yanai *et al.* (2000), a first cloud cluster reached the experiment site in mid-December and was accompanied by heavy rainfall, as shown in Figure 2. Convection slowed down around 25 December and diminished in early January. Then the cluster drifted further west and disappeared near 170°W around 10 January. The next period is associated with the MJO suppressed phase and is characterized by moderate precipitation. Finally, a second cluster reached the site in early February, resulting in intense convection during this month but in less precipitation than in December. The staged convective development associated with the MJO is detailed well in Kikuchi and Takayabu (2004).

The analysis of MJO periods by Chen *et al.* (1996), confirmed by the convection analysis in our simulations, leads us to define the two periods as follows: from 20 December 1992–5 January 1993 for the active phase and from 6 January 1993–26 January 1993 for the suppressed phase.

In order to study the contribution of convective scavenging in comparison with that of stratiform scavenging and the interaction of both convective and stratiform clouds with tracer distribution, two simulations are made without and with convective scavenging, hereafter referred to as simulations A and B, respectively. Another simulation is made without scavenging by stratiform precipitation and clouds (simulation C), in order to single out the role of convective transport. All the simulations are made on the whole TOGA–COARE experiment.

The three simulations are detailed in Table 1. All simulations take into account the removal of radionuclide tracers by radioactive decay, dry deposition (the dry deposition flux to the ground is assumed to be proportional to the aerosol concentration in the lowest model layer and to a velocity set to 0.1 cm s^{-1}) and transport by convective draughts.

The simulations are illustrated in Figure 2, showing the ^{7}Be concentration time series simulated for the two periods. Simulated

Table 1. Simulations and model parameters used in the simulations.

Simulation	Convective clouds	Stratiform clouds
A	Transport by air	In-cloud scavenging, impaction by rain
B	Transport by air, in-cloud scavenging, impaction by rain	In-cloud scavenging, impaction by rain
C	Transport by air, in-cloud scavenging, impaction by rain	None

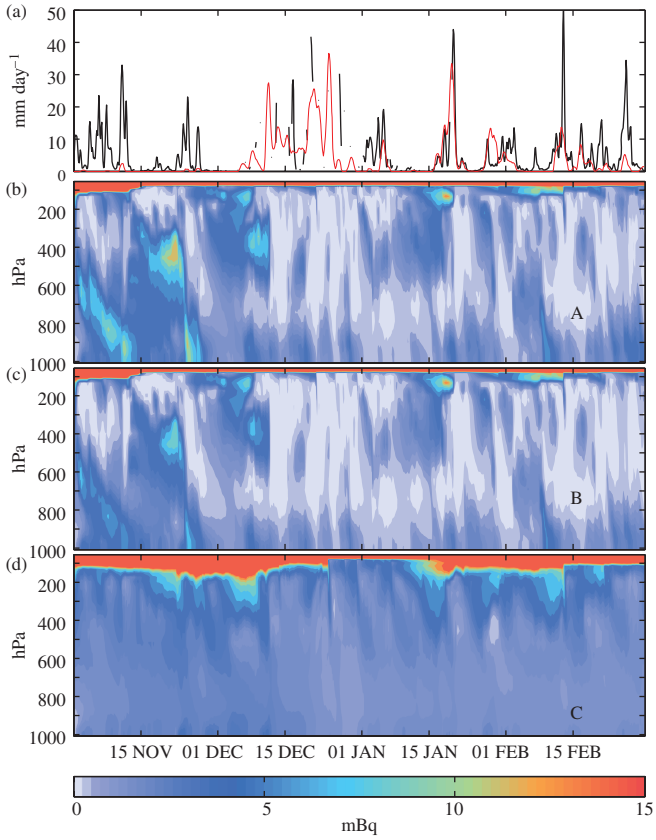

Figure 2. (a) Observed surface precipitation (black line) and simulated stratiform precipitation (red line) (mm day^{-1}) over the four months of TOGA–COARE. Considering how the forcing in the SCM is made, the simulated surface precipitation is consistent with the observed one and the difference between the red and black lines gives approximatively the convective precipitation. (b)–(d) ^{7}Be concentrations (mBq kg^{-1}) simulated by LMDz SCM in simulations A, B and C (see Table 1). Above 33 mBq kg^{-1}, details of the concentrations are not shown, in order for concentrations of the lower atmosphere to be displayed.

concentrations in Figure 2 show large temporal variations from the surface to the top of the troposphere and large differences between the three simulations in the whole troposphere. This highlights a strong cleansing by large-scale clouds and associated precipitation. Thereafter, only simulation B is studied in detail, but the vertical profile of the tracer is compared with the two other simulations.

The analysis of these results is based on the following.

1. The comparison of the vertical distributions of simulated precipitation fluxes between the two periods (Figure 3).
2. The comparison of tracer concentrations between simulations A and B (Figures 4(a) and 5(a), right) and of tracer tendencies (Figures 4(a), 5(a), left) for each period. Convective tracer tendencies in the saturated draughts and unsaturated downdraught are represented separately. Both include the effect of precipitation and their sum is equal to the total convective tendency as defined in Eq. (1). Over the entire troposphere, the tendency induced due to convective saturated draughts is owed almost entirely to the last two terms of Eq. (10a), namely the compensating subsidence and the scavenging terms (not shown). The large-scale tendency is separated into nucleation and impaction tendencies. The effect of large-scale precipitation evaporation is the difference between the total tendency and nucleation and impaction tendencies.
3. The comparison of the convective mass fluxes between the two periods (Figures 4(b) and 5(b)). The analysis is focused on the effect of both convection and large-scale precipitation on the tracer distribution. The contribution of other processes is not discussed.

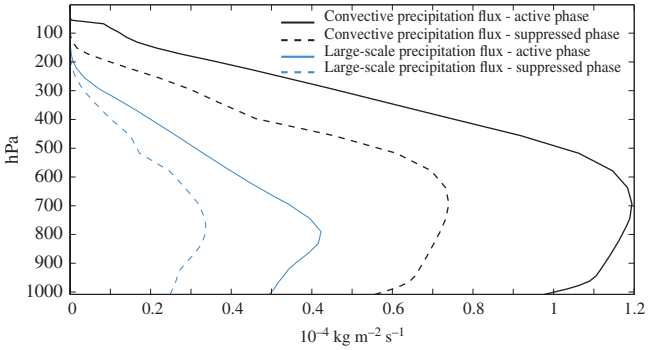

Figure 3. Simulated vertical profiles of convective (black) and large-scale (blue) precipitation flux (10^{-4} kg m^{-2} s^{-1}) during the active phase (solid line) and the suppressed phase (dashed line).

Convection intensity is closely related to precipitation fluxes as shown in Figure 3, where the suppressed phase, in the absence of a cluster, is characterized by low values of these fluxes from the surface to the top of the cloud, which is located around 18 km. The vertical precipitation flux gradient is also an indicator of precipitation behaviour. A positive vertical gradient is associated with the evaporation of rain, which is likely to release tracers. For both phases, this positive gradient is the largest between the surface and 950 hPa.

3.3.1. *Active phase*

The active phase is characterized by heavy rainfall (Figures 2 and 3) and large convective fluxes (Figure 4(b)). The cloud top is located above 100 hPa, where all mass fluxes become negligible. Whilst tendencies induced by large-scale and convective clouds and precipitation are of the same order of magnitude, adding the convective scavenging leads only to a 20–30% decrease of ^{7}Be concentration (Figure 4(a), right). At the base of the atmosphere, tracer release by precipitation evaporation increases the concentration.

In the upper troposphere (between 50 and 500 hPa), both large-scale and convective total tendencies are negative: large-scale condensation of water removes, by nucleation, tracers from the environment, while at these levels deep convection detrains low-level air with low ^{7}Be concentration. Large-scale clouds release tracer at lower levels by evaporation of their precipitation (mostly around 450 hPa), where the difference between the large-scale total tendency and in-cloud large-scale scavenging tendency is largest.

Between 500 and 800 hPa, large-scale clouds still remove tracer by nucleation, whereas deep convective processes tend to increase concentrations. The compensating subsidence (since the tendency induced by the saturated draughts is almost equal to the total convective tendency) explains most of the positive total convective tendency; it brings down high concentrations from the upper troposphere to altitudes where the concentrations are lower (Figure 4(a), left).

Below 800 hPa, the conversion to precipitation is very weak in convective saturated draughts, so that the convective tendency is only due to the effect of the compensating subsidence and the unsaturated downdraughts. The vertical gradient of ^{7}Be

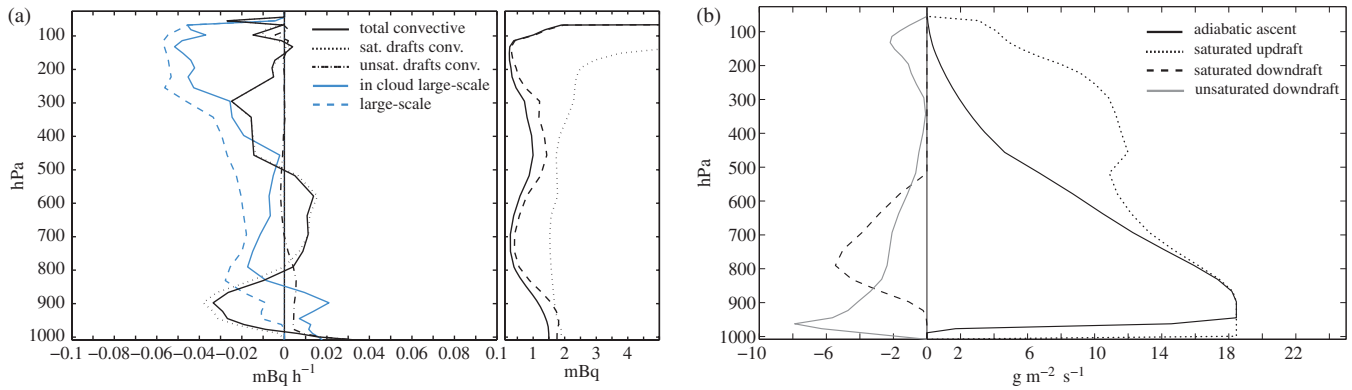

Figure 4. Active phase. (a) *Left:* simulated vertical tendencies (mBq kg^{-1} h^{-1}). The total convective tendency of simulation B (solid black line) is separated into two tendencies: saturated draughts with scavenging (black dotted line), unsaturated downdraught (black dashed line), total large-scale tendency (blue solid line) and in-cloud scavenging tendency (blue dashed line) (impaction scavenging is negligible and the effect of evaporation is the difference between in-cloud scavenging and total tendencies). *Right:* the vertical profile of ^{7}Be concentration (mBq kg^{-1}) of simulations A (dashed line), B (solid line) and C (dotted line). (b) Simulated convective mass fluxes (g m^{-2} s^{-1}): adiabatic ascent (solid black line), saturated downdraught (dashed line), saturated updraught (dotted line) and unsaturated downdraught (grey line).

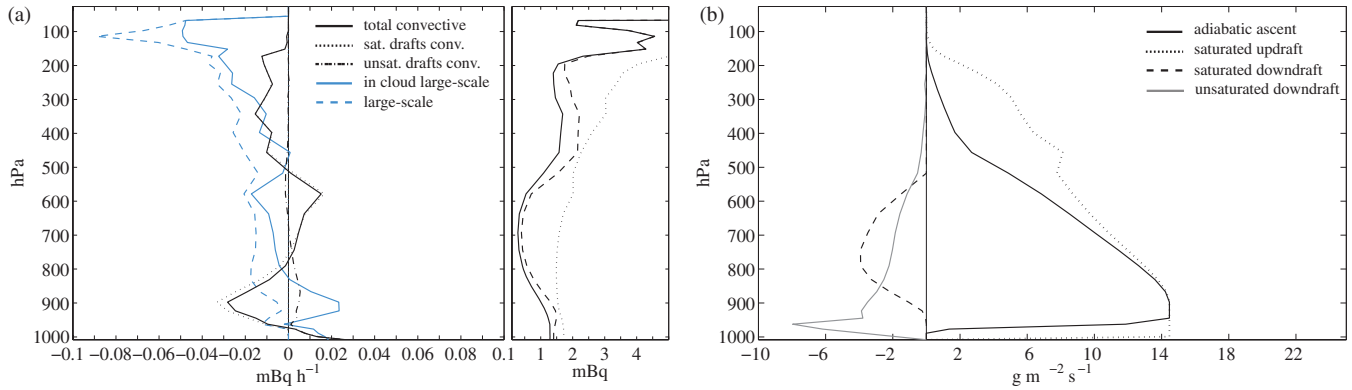

Figure 5. Suppressed phase during TOGA–COARE. (a) The same as Figure 4(a). (b) The same as Figure 4(b).

concentration is 0 in the well-mixed boundary layer (below 950 hPa) and negative above and so is the tendency due to saturated draughts. The tendency due to the unsaturated downdraught is weak above cloud base (950 hPa) and large below, where precipitation evaporates at a high rate and the mass flux of the downdraught is strongly diverging (Figure 4(b)). This tendency increases rapidly close to the surface, reaching values as high as 0.03 mBq kg^{-1} h^{-1}.

Scavenging in large-scale clouds decreases from 800 to 950 hPa, where it reaches zero, but the decrease is not regular: precipitating clouds form between 900 and 950 hPa. This cloud layer is associated with a minimum of relative humidity around 900 hPa (not shown), which yields the maximum evaporation of large-scale rain at 900 hPa.

Impaction by convective precipitation has little effect regarding the size of the aerosols to which ^{7}Be is attached, the size of the raindrops in the model and the respective collision efficiency. Impaction scavenging by large-scale precipitation is very low (close to zero) compared with the other tendencies, although we use the same raindrop size as for convective rain.

The mean wet deposit due to convective and large-scale precipitation is 1739 and 7531 mBq m^{-2} day^{-1}, respectively.

3.3.2. *Suppressed phase*

This period with weaker convection is characterized by moderate precipitation (Figure 2) and smaller convective fluxes (Figure 5) compared with the active phase. Most of the above-mentioned processes are present but are attenuated, as illustrated in Figure 5. Scavenging of tracers occurs between the top cloud and 500 hPa (Figure 5(a), left) and is caused mainly by nucleation in large-scale and convective clouds. Precipitation of the unsaturated downdraught also removes tracers from the environment.

Between 500 and 750 hPa, the compensating subsidence brings down rich concentrations and the tendency induced by the convection is positive. Below, between 750 and 900 hPa, the compensating subsidence brings down poor concentrations and the tendency induced by the convection is thus negative. Below 800 hPa, tracer release by evaporation in the unsaturated downdraught and by evaporation of large-scale precipitation yields larger concentrations of tracers, as shown in Figure 2 and the left part of Figure 5(a). At the surface, this process produces a positive peak of the tendency in the unsaturated downdraught (Figure 5(a), left) and equals the positive tendency produced by the large-scale precipitation evaporation. Release of tracers by evaporation also has a larger effect, in this phase, than compensating subsidence. Again, impaction scavenging is negligible.

The mean wet deposit due to convective and large-scale precipitation is 928 and 6226 mBq m^{-2} day^{-1}, respectively.

3.3.3. *Relative significance of processes at the surface*

The mean convective and large-scale tendencies in Figures 4 and 5 show that the tracer distribution is dependent on convective transport and scavenging as well as scavenging by large-scale clouds and associated precipitation. In the planetary boundary layer (PBL), both of the tendencies are positive (Figures 4 and 5) during the active and suppressed phases and of the order of magnitude 0.5 mBq kg^{-1} day^{-1}, i.e. 15 mBq kg^{-1} month^{-1}. In contrast, the mean surface concentration stays below 2 mBq kg^{-1} (Figures 4(a), 5(a), right). This results from a balance between the removal of tracer by entrainment into the saturated updraught, redistribution of the PBL in the upper layers of the troposphere and addition of tracers by evaporation of both convective and large-scale precipitation.

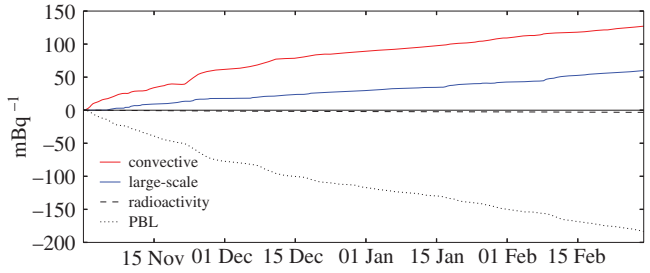

Figure 6. Cumulative tendencies in the first layer of the model (thickness $z_1 = 70$ m) induced by convection (red), large-scale precipitation (blue), boundary-layer (dotted line) and radioactive decay (dashed line) in the TOGA–COARE case (simulation B). The boundary-layer tendency in the first model layer ($(\partial_t C_1)_{bl}$) results from the balance between the dry deposit (Φ_d) and the turbulent flux at the layer top (parametrized as vertical diffusion with eddy diffusivity K_z: $\rho z_1(\partial_t C_1)_{bl} = -\Phi_d + K_z(\partial_z C)(z_1)$).

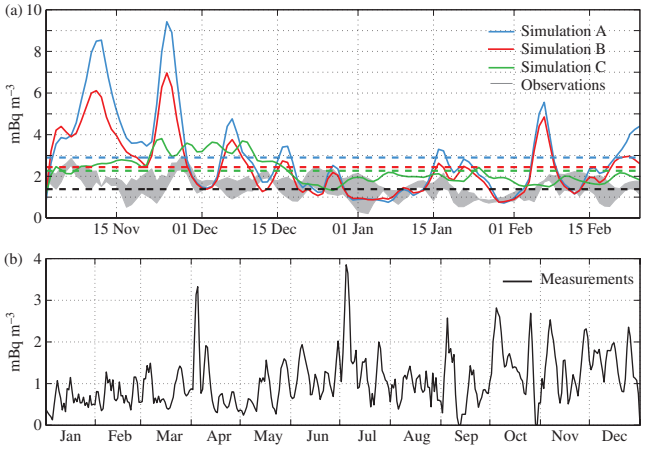

Figure 7. (a) Comparison of the daily simulated ^{7}Be surface concentrations (blue: simulation A; red: simulation B; green: simulation C) and the CTBTO interannual minimum and maximum of the observations (the lower part of the shaded area corresponds to the minimum value of the data for each day and the upper part corresponds to the maximum value) associated with their mean values, shown as dashed lines, over the four months of TOGA–COARE. (b) Surface concentrations of ^{7}Be for 2007 measured at the IMS station located at 150°E, 3°S.

Cumulative tendencies (Figure 6) underline the predominance of the effects of deep convection on tracers close to the surface during the whole experiment, despite the alternation of MJO phases: the convective tendency is larger by a factor of two compared with the large-scale tendency. The tendency induced by processes occurring in the PBL (dotted line in Figure 6) is equal to the opposite of the sum of large-scale and convective tendencies (blue and red lines in Figure 6). Thus, the PBL balances effects induced by mechanisms associated with deep convection and large-scale clouds. It should be noted that, in the case where scavenging by convective processes is not active (simulation A), large-scale tendencies predominate over convective tendencies in the PBL.

The average wet deposit over the whole TOGA–COARE period is 1392 and 4405 mBq m^{-2} day^{-1} for the convective and large-scale precipitation, respectively.

3.3.4. *Comparison with observations*

Simulated ^{7}Be surface concentrations are compared with daily averaged concentrations measured by a station located in Kavieng (150°E, 3°S), Papua New Guinea, close to the TOGA–COARE Intensive Field Array. This station belongs to the International Monitoring System (IMS), developed in the framework of the Comprehensive Test Ban Treaty. The station has been measuring airborne aerosols and particles with very low-level radioactivity (Schulze *et al.*, 2000) since 2007. Measurements are erratic (there are no data during 2008, the first two months of 2010 and the second half of 2011). Nevertheless, as the interannual variability of ^{7}Be surface concentration is of the order of the day-to-day variability, we compare simulations with interannual mean values and spread. Hence, Figure 7 presents the comparison between TOGA–COARE simulations with observations available between 2007 and 2011 over the four months NDJF.

The main feature of deep convective transport associated with ^{7}Be is to displace these tracers from the upper troposphere and to bring them down to lower layers of the atmosphere. Moreover, concentrations within the PBL are enhanced as a result of tracer release by evaporation of convective and large-scale precipitation, the effect of the latter being dominant.

The mean values of the simulated surface concentrations with convective scavenging (2.42 mBq m^{-3}) are lower than those simulated without convective scavenging (2.90 mBq m^{-3}), approaching the mean value of interannual observations (1.38 mBq m^{-3}). The mean simulated surface concentrations in simulation C, without scavenging by stratiform clouds and rain (2.26 mBq m^{-3}), are the lowest ones. In simulation A, the absence of removal by convective precipitation is compensated for by a stronger wet removal by stratiform precipitation: stratiform precipitation, containing a higher ^{7}Be concentration, liberates more tracers when evaporating in the PBL than in simulation B.

Peaks in simulations A and B around 10 and 25 November can be related to the large-scale nucleation in the upper troposphere as well as to release in the lower layers by the evaporation of precipitation, which results in the downward transport of the tracer to the surface. These peaks are higher than the range of measured concentrations (Figure 7(b)) but are, however, in the range of measured concentrations at other stations where MJO events occur (not shown here). It is worth noting that large-scale and convective scavenging can, by itself, lead to a similar mean surface concentration and variability (Figure 7: blue and green lines). During the heavy rainfall in the second half of December, large-scale precipitation cleans the troposphere and reduces surface concentrations.

As shown by the evident decrease of surface concentrations during the active phase (from 12 December until the half of January), tracers are scavenged more when heavy rainfall occurs, i.e. during MJO active phases. Conversely, during suppressed phases, light precipitation occurs and tracer concentration is higher.

4. GCM simulations

In the GCM, subgrid-scale processes are solved for each column separately, making it possible to use the new parametrization (sections 2.1 and 2.2) in the three-dimensional model. The 3D approach has the advantage of being able to simulate the transport of terrestrial radionuclides such as ^{210}Pb, which was not the case in the SCM owing to the specific conditions at the surface.

The source of ^{210}Pb atoms is the radioactive decay product of ^{222}Rn, which is emitted in the model from a soil reservoir 10 cm thick. The emission flux of ^{222}Rn is prescribed to 1 atom cm^{-2} s^{-1} on the continents. Because of their respective lifetimes (3.8 days for ^{222}Rn and 22 years for ^{210}Pb), ^{210}Pb particles are continuously formed in the first layers of the model.

A two-year climate simulation and one-year simulation with nudged horizontal winds have been performed in order to characterize the vertical distribution of the radionuclides and to compare the results with radionuclide observations from IMS stations, respectively. Both simulations use the parametrization of section 2, while the climate simulation uses the same parameters as in simulation B in section 3.

We use two parametrizations of large-scale scavenging. The first one (Genthon, 1992) is identical to the one used in Heinrich and Jamelot (2011) and has been developed to study the transport of dust and sea-salt aerosols over the Antarctic. This scheme does not take into account release by the evaporation of stratiform precipitation. We shall use it when comparing our simulations with those of Heinrich and Jamelot (2011) in order to assess the effect of the representation of convective scavenging. The second

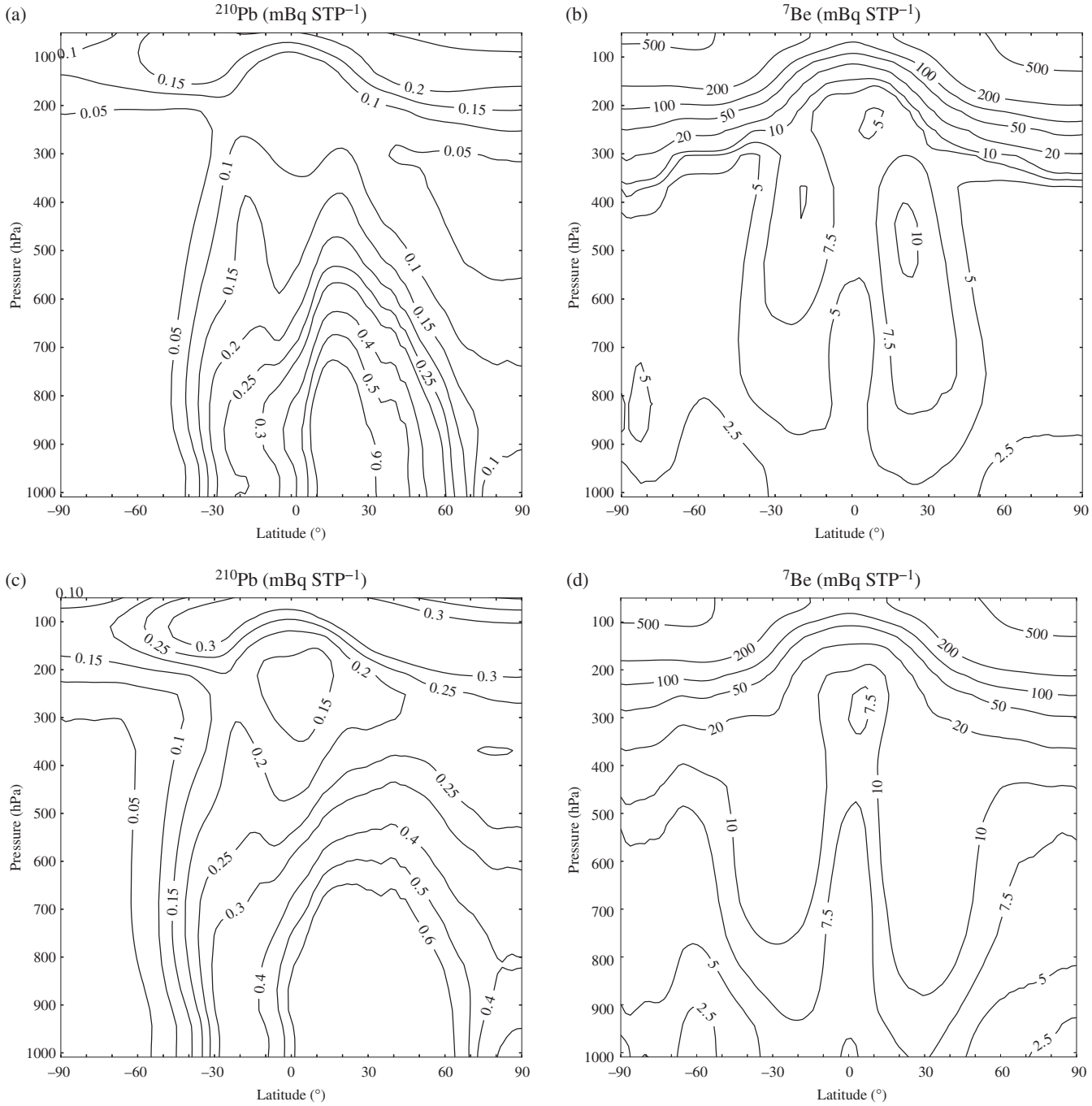

Figure 8. Zonal average of (a) ^{210}Pb and (b) ^{7}Be concentrations in mBq per unit of volume at the standard conditions for temperature and pressure (STP). 1 mBq STP^{-1} = 1.3 mBq kg^{-1} approximately, using a fraction of aerosols in the aqueous phase of large-scale clouds set to 70%, as in Reddy and Boucher (2004) (see the Appendix for the various definitions of the aqueous phase). (c) and (d) The same as (a) and (b), except that the fraction of aerosols in the aqueous phase of large-scale clouds is lowered to 10%.

one, already used in 1D simulations of the TOGA–COARE case, follows more closely the physical processes represented in the GCM and will be used for climatological simulations.

The GCM simulations have been performed with a horizontal resolution of 3.75° in longitude and 1.875° in latitude. On the vertical, the model uses, as the SCM version, 39 levels.

4.1. *Climate simulations*

4.1.1. *Vertical distribution*

To characterize better the performance of the new scheme and to highlight the significant role of large-scale processes in tracer distribution, the zonal mean of the concentrations of ^{210}Pb and ^{7}Be, averaged over the two years of climate simulations (1983 and 1984), is shown in Figure 8. Here, the radionuclide concentrations are expressed in mBq per standard cubic metre to be comparable with the literature.

Figure 8(a) shows, as reported by Giannakopoulos *et al.* (1999) and Liu *et al.* (2001), a minimum ^{210}Pb concentration located in the upper tropical troposphere. Nucleation scavenging in deep convective clouds causes this minimum and can correlated with the ^{7}Be minimum concentration (Figure 8(b)). Over the southern midlatitudes, values of ^{210}Pb concentration are higher than those from Liu *et al.* (2001) and are attributed to large-scale nucleation scavenging, which is likely less efficient in our model.

^{7}Be concentrations emphasize the Hadley circulation, with its dry descending branches over the Tropics.

Figure 8(c) and (d) represent a simulation in which we have reduced the large-scale nucleation scavenging coefficient to 10%, compared with 70% (RB04), in order to decrease the effect of scavenging in large-scale clouds, particularly in the upper troposphere, as mentioned by Croft *et al.* (2010) and suggested by the high surface concentration induced by this process in the TOGA–COARE case results (section 3.3.4). Since our model does not distinguish ice nucleation from liquid nucleation, the

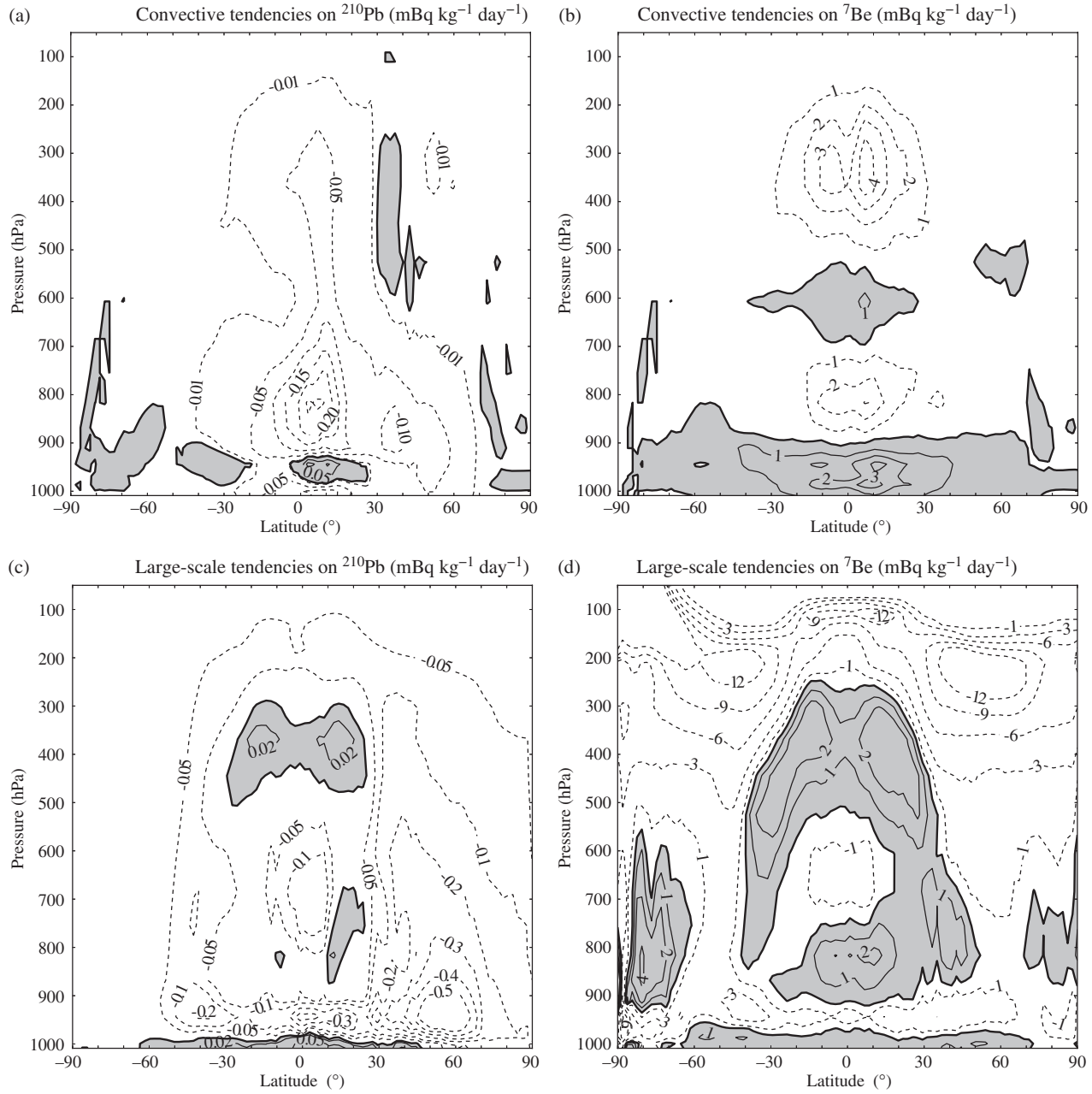

Figure 9. Simulated vertical tendencies of ^{210}Pb (left panels) and ^{7}Be (right panels) (mBq kg^{-1} day^{-1}) in the climate simulation, induced by (a) and (b) convection and (c) and (d) large-scale processes. The thick line represents 0 mBq kg^{-1} day^{-1} and grey areas correspond to positive tendencies.

large-scale nucleation scavenging coefficient (given by α in the Appendix) is reduced to 10% for all clouds (whether liquid, ice or mixed). Assuming that large-scale nucleation scavenging is as inefficient in liquid clouds as in ice clouds is unphysical. For instance, measurements by Henning *et al.* (2004) established that, for aerosols in the accumulation mode, the in-cloud scavenging coefficient is lower in ice and mixed-phase clouds than in warmer clouds, i.e. lower than 0.2. While this approximation may affect quantitative results, we assume that it does not change the main features of the radionuclide distributions significantly. However, in this version of LMDz, low-level clouds are underestimated (Hourdin *et al.*, 2006), thus the effect of this assumption is lightened for liquid clouds. The point is discussed further in the conclusion.

In Figure 8(a) and (b), concentrations are lower than those of Liu *et al.* (2001) in the free troposphere and do not have the same patterns as in Liu *et al.* (2001). When scavenging by large-scale nucleation is reduced, general patterns are closer than in the aforementioned study. In Figure 8(c), it is worth noting that the ^{210}Pb concentration is uniformly low over the southern high latitudes ($< -50°$) between the surface and 200 hPa. This is attributed to the scavenging associated with the large fraction of large-scale clouds present in the simulation at these latitudes (not shown).

Both of the radionuclide zonal distributions are consistent with the simulations of Liu *et al.* (2001).

4.1.2. *Effect of processes on radionuclide distributions*

The effects of deep convection and large-scale processes on the climate simulation, using a large-scale nucleation scavenging coefficient of 10%, are shown in Figure 9. Tendencies for the simulation with a large-scale nucleation scavenging coefficient of 70% are not shown: the spatial distribution of tendencies is quite similar, but the tendencies have a different magnitude.

4.1.2.1. *^{210}Pb*

While deep convection mainly impacts ^{210}Pb concentrations in the Tropics (Figure 9(a)), large-scale clouds affect its concentration mostly in midlatitudes and at lower altitudes, the boundary layer included (Figure 9(c)). Over Antarctica (Figure 9(c)), tendencies are weak and negative (except for some positive tendency due to shallow convection), which is consistent with the very low concentrations in this region.

In the Tropics, all tendencies are negative above 300 hPa: ^{210}Pb is brought above these levels by the ascending branch of the Hadley cells; there it is removed by both large-scale nucleation and convective scavenging. A part of the scavenged ^{210}Pb is released between 300 and 500 hPa by evaporation of stratiform precipitation.

In the Tropics, convective tendencies are mainly negative (Figure 9(a)), which means that all the ^{210}Pb lifted in convective updraughts is removed by convective scavenging. Because the conversion into precipitation is very efficient in convective saturated draughts, most of the entrained radionuclides are transferred into convective precipitation. Convective precipitation evaporates in the low troposphere and releases the radionuclide between 900 and 975 hPa. However, the convective tendency is negative close to the surface: owing to the compensating subsidence, this process brings down low-concentration air at levels where the concentration is higher because of the terragenic source of ^{210}Pb.

4.1.2.2. ^{7}Be

Figure 9(b) shows that deep convection affects ^{7}Be concentrations predominantly in the Tropics, with a behaviour similar to that observed in the SCM simulation (Figures 5 and 4), but the magnitudes of the tendencies in the climate simulations are approximately threefold larger. In the upper troposphere (between 200 and 500 hPa), deep convection detrains low-level air with low ^{7}Be concentrations at these levels. Below 500 hPa, the conversion to precipitation is very weak in convective saturated draughts, so that the convective tendency is only due to the effects of the compensating subsidence and unsaturated downdraughts. Except in the PBL, in which tracers are released by evaporation of convective precipitation, the vertical gradient of ^{7}Be concentration is affected by large-scale processes, as shown by Figure 9(d).

Large-scale nucleation at high altitudes (between 50 and 400 hPa in the midlatitudes and between 50 and 250 hPa in the Tropics) removes the ^{7}Be radionuclide (Figure 9(d)). Below these altitudes, nucleation scavenging alternates successively with release by evaporation of stratiform precipitation.

Between 900 hPa and the surface, the large-scale tendency is essentially due to the release of tracers by the evaporation of precipitation.

4.1.3. Budgets

Annual global budgets of ^{7}Be and ^{210}Pb in climate simulations are given in Table 2. The tropopause is defined using the criterion of a 2 °C km^{-1} lapse rate as defined by the World Meteorological Organization.

In contrast to Liu *et al.* (2001)'s study, in our model the wet deposition is predominantly induced by large-scale processes. As expected, when reducing the fraction of aerosols in the aqueous phase in large-scale clouds, the convective scavenging increases, thus partly balancing the decrease of large-scale scavenging.

Table 2. Annual average global budgets and residence times of tropospheric ^{7}Be and ^{210}Pb in climate simulations for two large-scale in-cloud scavenging coefficients.

	^{210}Pb		^{7}Be	
Fraction of activated CCN	0.7	0.1	0.7	0.1
Source (g day^{-1})	37	37	0.25	0.22
From stratosphere	–	–	0.08	0.05
Within troposphere	37	37	0.17	0.17
Burden (g)	244	389	2.3	3.7
Sinks (g day^{-1})	37.4	37.1	0.25	0.22
Wet deposition				
Convective	10.4	15.6	0.04	0.06
Stratiform	27	21.5	0.17	0.11
Dry deposition	10^{-5}	10^{-5}	0.01	0.02
Radioactive decay	0.05	0.03	0.03	0.03
Residence time (day)	6.5	10.5	9.2	16.8

Residence times of ^{7}Be in the troposphere are 9.2 days in the standard simulation (the fraction of aerosols in the aqueous phase in large-scale clouds is 0.7) and 16.8 days when this fraction is reduced to 0.1. Reducing nucleation scavenging in large-scale clouds improves the ^{7}Be residence time, which is in the range of values from the literature: from 10–35 days (Shapiro and Forbes-Resha, 1976; Bleichrodt, 1978; Koch *et al.*, 1996). Residence times of ^{210}Pb are 6.5 and 10.5 days for the standard simulation and for the one with a reduced fraction of activated CCN, respectively. In both simulations, ^{210}Pb residence times are in the range of those from the literature.

4.2. Nudged GCM simulations

4.2.1. Evaluation with surface measurements

The GCM has been simulated over the year 2007. Concentrations have been initialized from those calculated by a three-month simulation, to avoid underestimation of concentrations compared with measurements during the first months of 2007. GCM horizontal winds are nudged toward analyzed six-hourly time wind fields of the European Centre for Medium-Range Weather Forecasts (ERA-Interim). As in the SCM study, simulations are performed turning on or off convective scavenging and results are compared with observations. Unlike SCM simulations, we use the large-scale scavenging parametrization of Genthon (1992), inspired by the one of Radke *et al.* (1980), in which nucleation and impaction scavenging are calculated by integrating the quantity of tracer scavenged by either condensation or precipitation impaction. Release by the evaporation of large-scale precipitation is not taken into account. The results of this simulation are illustrated in Figures 10 and 11 and apply only to these figures.

The goal here is not to validate or to calibrate the new parametrization but rather to test it on a global scale and particularly in tropical regions. Surface concentrations in the Tropics are illustrated (Figure 10) by daily averaged concentrations of ^{210}Pb and ^{7}Be at the IMS station of Tahiti (French Polynesia), which presented a nearly full set of observations during 2007.

As expected for stations located outside the InterTropical Convergence Zone (ITCZ), the main effect of convective scavenging is to decrease concentrations of both radionuclides over the entire year. In the absence of this process (red line in Figure 10), the yearly averaged concentrations of ^{210}Pb and ^{7}Be (0.18 and 7 mBq m^{-3}, respectively) are largely overestimated compared with observations (0.06 and 4 mBq m^{-3}). The new parametrization reduces concentrations of ^{210}Pb and ^{7}Be to 0.10 and 5 mBq m^{3}, respectively, which are close to the results of Heinrich and Jamelot (2011). In contrast to the TOGA–COARE case, aerosol release by evaporation of convective precipitation is not dominant at this station, as confirmed by the analysis of tracer tendencies. Maps of concentrations (not shown) emphasize the major role of evaporation within the ITCZ, which yields high peaks of ^{7}Be during intense convective periods.

4.2.2. Tracers in precipitation

Several studies have investigated the concentration of ^{7}Be in precipitation. Ayub *et al.* (2009) have measured ^{7}Be content in precipitation in central Argentina, in a semi-arid and subtropical region. They measured an annual concentration of around 1.7 Bq L^{-1}, i.e. 10^{4} atom g^{-1}, with summer and winter ^{7}Be concentrations in precipitation of around 2 Bq L^{-1} (1.2×10^{4} atom g^{-1}) and around 1 Bq L^{-1} (0.6×10^{4} atom g^{-1}), respectively. The model reproduces a similar annual concentration in central Argentina (10^{4} atom g^{-1}), although the seasonal cycle of ^{7}Be concentrations in precipitation is the opposite of

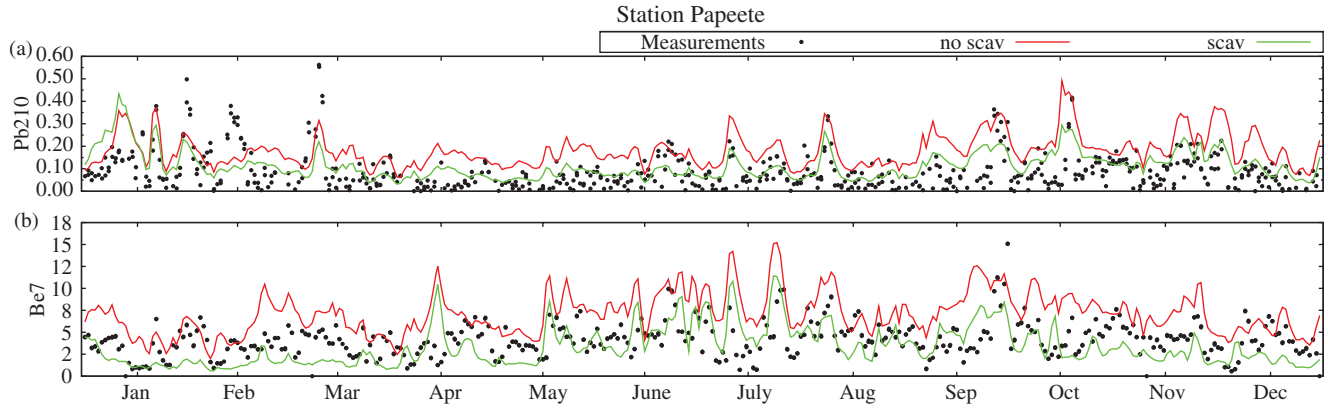

Figure 10. (a) and (b) Time series for the year 2007 of daily measured concentrations (dots) and simulated daily concentrations in mBq m^{-3} of (a) ^{210}Pb and (b) ^{7}Be (red line: without convective scavenging; green line: with convective scavenging) at Tahiti station.

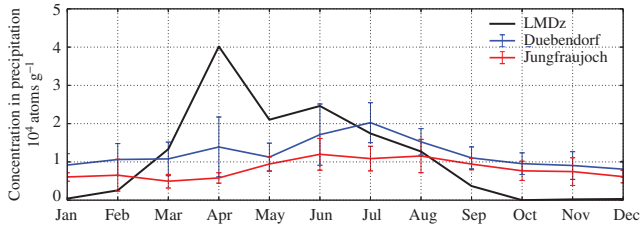

Figure 11. Concentration in precipitation of ^{7}Be measured by Heikkilä *et al.* (2008), averaged over eight years (1998–2005), at Jungfraujoch (blue) and at Dübendorf (red) in Switzerland, together with the simulated concentration (black) in convective precipitation for 2007 at the same location (owing to the LMDz GCM resolution, both of the locations are in the same grid cell).

the observations (0.9×10^4 and 2×10^4 atom g^{-1} for summer and winter concentration, respectively). It is explained by rare and mainly stratiform winter precipitation and by summer precipitation that is entirely convective at this location.

Kadko and Prospero (2011) have measured ^{7}Be concentrations in precipitation in the Bermudas and found an annual concentration of $1.2 \times 10^4 \pm 0.5 \times 10^4$ atom g^{-1}. In LMDz, at this location, the value is 0.9×10^4 atom g^{-1}, which is in the range of the observations.

^{7}Be concentration in precipitation has also been measured by Heikkilä *et al.* (2008) over Switzerland. Simulated ^{7}Be monthly concentrations in precipitation at those locations are compared with observations and are shown in Figure 11. The mean values of the observations at Jungfraujoch and Dübendorf are 8200 and 12 200 atom g^{-1}, respectively, which is in the range measured by Ayub *et al.* (2009) and Kadko and Prospero (2011) at different locations.

Heikkilä *et al.* (2008) conclude that the seasonality of the measured radionuclide is similar to the precipitation rate, which allows us to compare the concentrations of ^{7}Be with their measurements. Owing to the duration of the three-dimensional simulation, we look at the ^{7}Be concentrations in precipitation of the nudged simulation at the same location in Switzerland. Simulated concentrations are shown in Figure 11.

The annual cycle is well captured, despite the fact that the large-scale scavenging parametrization (Genthon, 1992) used in the simulation does not provide the tracer concentration in large-scale precipitation. Concentrations are larger and of the same order of magnitude during summertime. Concentrations are low (almost zero) during wintertime. The large amount of tracer in precipitation during summer is correlated with the simulated precipitation (not shown here), which is mostly convective during this period. Furthermore, the concentration peak in April is correlated with a high ^{7}Be concentration owing to a low tropopause. Hence, convective clouds displaced high ^{7}Be concentrations to the surface through precipitation.

5. Conclusions

A new parametrization of aerosol scavenging has been implemented in Emanuel's deep convective scheme. It makes it possible to analyze separately the effects of various components of the convective process on the concentration of tracers attached to aerosols: transport in convective draughts, scavenging in saturated draughts, the redistribution of aerosols by detrainment and precipitation evaporation and the elimination of aerosols by precipitation. Transport and scavenging have been evaluated using the single-column version of the LMDZ GCM in simulations of a four-month TOGA–COARE case over the ocean. Thanks to its high troposphere origin and its lifetime (53 days), which is longer than the studied processes, ^{7}Be is an ideal tracer for investigating the mechanisms that move aerosols downwards: precipitation processes, convective compensating subsidence and convective unsaturated downdraughts. Without these processes, concentrations of ^{7}Be in the troposphere and particularly at the surface should be lower than a few mBq m^{-3}.

The simulated mean concentrations of ^{7}Be are of the same order of magnitude as those of the observations over the four-month period, which allows their use to aid better understanding of the respective roles of processes responsible for the vertical distribution of ^{7}Be.

It appears that the effect of large-scale cloud formation and related precipitation processes interacts strongly with the effect of deep convection processes. SCM results indicate that in-cloud scavenging, by both convective and large-scale processes, plays a significant role in high tropospheric tracer distribution, with a strong negative tendency. In contrast, below-cloud evaporation plays a significant role in surface concentration with a strong positive tendency. The compensating subsidence of deep convection, by bringing down air rich in ^{7}Be, has a positive effect on tracer concentration in the mid-troposphere. Large-scale clouds also move tracers down, after successive nucleation and evaporation of precipitation. Convective impaction has a minor impact on environmental tracers and impaction from large-scale precipitation is negligible for these simulations.

Overall, large-scale nucleation scavenging appears to be more efficient to clean the atmosphere than moist convection. Large-scale scavenging has a major influence on aerosol cleansing in the troposphere, especially in the upper troposphere; tracer release by evaporation of convective precipitation dominates in the PBL. Zonal and vertical distributions of ^{7}Be and ^{210}Pb indicate the significance of large-scale nucleation in the tracer distribution. Reducing the efficiency of large-scale nucleation improves zonal and vertical distributions of ^{7}Be and ^{210}Pb in our simulations. However, large-scale removal processes still need to be studied, since, in our model, the large-scale nucleation does not differentiate ice nucleation from water nucleation, which is not consistent with the formulation of large-scale precipitation in LMDZ. This last result could arise from compensating errors

from both the scavenging schemes and the large-scale clouds and precipitation scheme, as well as from the model underestimation of low-level clouds. It is also possible that, in LMDz, large-scale clouds and precipitation are too dominant and replace convection. At any rate, the first improvement of the model in future simulations will be to introduce a phase dependence for the large-scale nucleation coefficient.

This study only focused on oceanic moist convection. Continental convection displays deeper and more intense updraughts. Moreover, it is expected to yield stronger low-level evaporation. Both features should make the role of deep convection more prominent over land than over ocean.

As 3D GCM simulations are likely to represent the intricacy of tropical convective systems better, the new scheme has also been introduced and tested in the atmospheric general circulation model LMDz, using two natural radionuclides, ^{210}Pb and ^{7}Be. Due to their opposite sources, this couple of radionuclides should provide constraints on the parametrization of convective scavenging. Preliminary results encourage us to carry on the validation and calibration of this parametrization in the GCM.

Appendix A: Parameterizations of the large-scale scavenging

A1. The original Preiss and Genthon parametrization

Genthon (1992) defined a wet deposition model for stratiform precipitation, based on the model of Giorgi and Chameides (1986), but expressed the large-scale nucleation and impaction scavenging coefficients differently.

If $\tilde{C}$ is the mass concentration of the tracer, its variation $\delta_t\tilde{C}$ over a time increment δt reads

$$\delta_t\tilde{C} = \lambda_{LS}\,\tilde{C}\,, \tag{A1}$$

with $\lambda_{LS} = (1 - e^{-\eta Q})$ the scavenging coefficient and $Q = P\,\delta t$, where P (in $\mathrm{kg\,m^{-2}\,s^{-1}}$) is the precipitation flux (calculated at each level of the model) and η is a coefficient expressed in $\mathrm{m^2\,kg^{-1}}$. According to Radke *et al.* (1980), η depends on the scavenging (nucleation or impaction) and precipitation (liquid or solid).

Preiss and Genthon (1997) suggest that the coefficient η should be much weaker for impaction than for nucleation scavenging and they test the values 1 and 0 for nucleation and impaction scavenging. In our simulations, we do not distinguish between solid and liquid precipitation and set η to 0.75 and $0.5\,\mathrm{m^2\,kg^{-1}}$ for nucleation and impaction scavenging, respectively.

A2. The modified Reddy and Boucher parametrization

A2.1. In-cloud scavenging

In-cloud scavenging is assumed equal to $\beta f \alpha$ within each model layer, where f is the cloud fraction defined by Le Treut and Li (1991), α is the fraction of tracer in the aqueous phase (set to 0.7 in RB04) and β is the rate of conversion of cloud water to rain water. If S_P is the amount of precipitation formed per unit mass of air and q_l the amount of condensed water per unit mass of air, then $\beta = S_P/q_l$. In order to compute β, RB04 estimate S_P from the precipitation divergence, while the amount of condensed water is determined from the cloud cover and a prescribed in-cloud water content q_{l0} (set to $0.5\,\mathrm{g\,kg^{-1}}$): $q_l = f q_{l0}$. In our modified version, we follow the large-scale condensation parametrization more closely: we compute β directly within this parametrization, where q_l and S_P are available at every time step, every level and every grid cell.

A2.2. Impaction

Impaction is dealt with in a fashion similar to the impaction by convective precipitation (section 2.5), although the precipitation is not correlated to any precipitation fraction, in accordance with Reddy and Boucher (2004). At each grid point, impaction scavenging is parametrized by integrating the volume swept by falling raindrops in the layer k:

$$\left(\partial_t\tilde{C}\right)_{\mathrm{imp},LS} = -\Lambda_{LS}\,\tilde{C}_k\,. \tag{A2}$$

The scavenging coefficient Λ_{LS} reads

$$\Lambda_{LS} = \mathcal{E}_{LS}\,\frac{3\,(P_k + P_{k+1})/2}{4\,\rho_l\,r}, \tag{A3}$$

where $\mathcal{E}_{LS}$ is the impaction efficiency, set to 10^{-3} and 10^{-2} for raindrops and snowflakes respectively based on measurements compiled by Pruppacher and Klett (1996), and r the mean raindrop radius (set to 1 mm by Reddy and Boucher, 2004).

A3. Release by evaporation

The concentration of tracer in the precipitation evaporated within a given layer k is assumed to be a fraction ν (set to 0.5 in RB04) of the concentration of tracer in the precipitation. RB04 and our modified version differ in the concentration used to compute this fraction: in RB04 it is the concentration $C_{p,k+1}$ in the precipitation entering the layer, while in our version it is the concentration $C_{p,k}$ in the precipitation within the layer k. Thus, in our version, the amount E_k of tracer released by evaporation within the layer k reads $E_k = \nu(P_{k+1} - P_k)\,C_{p,k}$ (where P_{k+1} and P_k are the precipitation fluxes at the upper and lower interfaces of layer k). Then, from tracer conservation, an expression for E_k in terms of P_{k+1} and $C_{p,k+1}$ follows:

$$E_k = P_{k+1}C_{p,k+1}\,\frac{\nu\,\gamma}{1 - \gamma\,(1 - \nu)}, \tag{A4}$$

where $\gamma = (P_{k+1} - P_k)/P_{k+1}$. With this equation, the case of complete evaporation is not a special case, since $E_k \to P_{k+1}C_{p,k+1}$ when $\gamma \to 1$. In contrast, RB04 (but also Liu *et al.*, 2001) must treat this case separately.

References

Andreae M, Rosenfeld D. 2008. Aerosol–cloud–precipitation interactions. Part 1. The nature and sources of cloud-active aerosols. *Earth Sci. Rev.* **89**: 13–41.

Ayub JJ, Gregorio DD, Velasco H, Huck H, Rizzotto M, Lohaiza F. 2009. Short-term seasonal variability in ^{7}Be wet deposition in a semiarid ecosystem of central Argentina. *J. Environ. Radioact.* **100**: 977–981.

Balkanski YJ, Jacob DJ, Gardner G, Graustein WC, Turekian KK. 1993. Transport and residence times of tropospheric aerosols inferred from a global three-dimensional simulation of ^{210}Pb. *J. Geophys. Res.* **98**: 20573–20586, doi: 10.1029/93JD02456.

Bleichrodt J. 1978. Mean tropospheric residence time of cosmic-ray-produced beryllium 7 at north temperate latitudes. *J. Geophys. Res.* **83**: 3058–3062, doi: 10.1029/JC083iC06p03058.

Bondietti E, Brantley J, Rangarajan C. 1987. Size distributions and growth of natural and Chernobyl-derived submicron aerosols in Tennessee. *J. Environ. Radioact.* **6**: 99–120.

Bony S, Emanuel K. 2001. A parameterization of the cloudiness associated with cumulus convection; evaluation using TOGA COARE data. *J. Atmos. Sci.* **58**: 3158–3183.

Bony S, Risi C, Vimeux F. 2008. Influence of convective processes on the isotopic composition (δ^{18}O and δD) of precipitation and water vapor in the Tropics: 1. Radiative–convective equilibrium and Tropical Ocean–Global Atmosphere–Coupled Ocean–Atmosphere response experiment (TOGA–COARE) simulations. *J. Geophys. Res.* **113**: D19305, doi: 10.1029/2008JD009942.

Chen SS, Houze RA Jr, Mapes BE. 1996 Multiscale variability of deep convection in relation to large-scale circulation in TOGA COARE. *J. Atmos. Sci.* **53**: 1380–1409.

Ciesielski PE, Johnson RH, Haertel PT, Wang J. 2003. Corrected TOGA COARE sounding humidity data: Impact on diagnosed properties of convection and climate over the warm pool. *J. Clim.* **16**: 2370–2384.

Croft B, Lohmann U, Martin RV, Stier P, Wurzler S, Feichter J, Hoose C, Heikkilä U, van Donkelaar A, Ferrachat S. 2010. Influences of in-cloud aerosol scavenging parameterizations on aerosol concentrations and wet deposition in ECHAM5-HAM. *Atmos. Chem. Phys.* **10**: 1511–1543.

Emanuel K. 1991. A scheme for representing cumulus convection in large scale models. *J. Atmos. Sci.* **48**: 2313–2329.

Emanuel K, Živković-Rothman M. 1999. Development and evaluation of a convection scheme for use in climate models. *J. Atmos. Sci.* **56**: 1766–1782.

Genthon C. 1992. Simulations of desert dust and sea-salt aerosols in Antartica with a general circulation model of the atmosphere. *Tellus* **44B**: 371–389.

Giannakopoulos C, Chipperfield MP, Law KS, Pyle JA. 1999. Validation and intercomparison of wet and dry deposition schemes using ^{210}Pb in a global three-dimensional off-line chemical transport model. *J. Geophys. Res.: Atmos.* **104**: 23761–23784, doi: 10.1029/1999JD900392.

Giorgi F, Chameides LW. 1986. Rainout lifetimes of highly soluble aerosols and gases as inferred from simulations with a general circulation model. *J. Geophys. Res.* **91**: 14367–14376, doi: 10.1029/JD091iD13p14367.

Greenfield SM. 1957. Rain scavenging of radioactive particulate matter from the atmosphere. *J. Meteorol.* **14**: 115–125.

Heikkilä U, Beer J, Alfimov V. 2008. Beryllium-10 and beryllium-7 in precipitation in Dübendorf (440 m) and at Jungfraujoch (3580 m), Switzerland(1998–2005). *J. Geophys. Res.* **113**, doi: 10.1029/2007JD009160.

Heinrich P, Jamelot A. 2011. Atmospheric transport simulation of ^{210}Pb and ^{7}Be by the LMDz general circulation model and sensitivity to convection and scavenging parameterization. *Atmos. Res.* **101**: 54–66.

Henning S, Bojinski S, Diehl K, Ghan S, Nyeki S, Weingartner E, Wurzler S, Baltensperger U. 2004. Aerosol partitioning in natural mixed-phase clouds. *Geophys. Res. Lett.* **31**, doi: 10.1029/2003GL019025.

Hourdin F, Musat I, Bony S, Braconnot P, Codron F, Dufresne J-L, Fairhead L, Filiberti M-A, Friedlingstein P, Grandpeix J-Y, Krinner G, LeVan P, Li Z-X, Lott F. 2006. The LMDZ4 general circulation model: Climate performance and sensitivity to parametrized physics with emphasis on tropical convection. *Clim. Dyn.* **27**: 787–813.

Hourdin F, Foujols M-A, Codron F, Guemas V, Dufresne J-L, Bony S, Denvil S, Guez L, Lott F, Ghattas J, Braconnot P, Marti O, Meurdesoif Y, Bopp L. 2012a. Climate and sensitivity of the IPSL–CM5A coupled model: Impact of the LMDZ atmospheric grid configuration. *Clim. Dyn.* **40**: 9–10 (Special issue).

Hourdin F, Grandpeix J-Y, Rio C, Bony S, Jam A, Cheruy F, Rochetin N, Fairhead L, Idelkadi A, Musat I, Dufresne J-L, Lahellec A, Lefebvre M-P, Roehrig R. 2012b. LMDZ5B: The atmospheric component of the IPSL climate model with revisited parameterizations for clouds and convection. *Clim. Dyn.* **40**: 1–30.

Jacob D. 2000. Heterogeneous chemistry and tropospheric ozone. *Atmos. Environ.* **34**: 2131–2159.

Kadko D, Prospero J. 2011. Deposition of ^{7}Be to Bermuda and the regional ocean: Environmental factors affecting estimates of atmospheric flux to the ocean. *J. Geophys. Res.* **116**: C02013, doi: 10.1029/2010JC006629.

Kikuchi K, Takayabu Y. 2004. The development of organized convection associated with the MJO during TOGA COARE IOP: Trimodal characteristics. *Geophys. Res. Lett.* **31**, doi: 10.1029/2004GL019601.

Koch D, Jacob D, Graustein W. 1996. Vertical transport of tropospheric aerosols as indicated by ^{7}Be and ^{210}Pb in a chemical tracer model. *J. Geophys. Res.* **101**: 18651–18666, doi: 10.1029/96JD01176.

Koch DM, Mann ME. 1996. Spatial and temporal variability of ^{7}Be surface concentrations. *Tellus B* **48**: 387–396.

Lal D, Peters B. 1967. Cosmic ray produced radioactivity on the Earth. In *Handbuch der Physik*, Sitte K. (ed.) 46: 551–612. Springer-Verlag: Berlin.

Lawrence MG, Rasch PJ. 2005. Tracer transport in deep convective updrafts: Plume ensemble versus bulk formulations. *J. Atmos. Sci.* **62**: 2880–2894.

Le Treut H, Li Z-X. 1991. Sensitivity of an atmospheric general circulation model to prescribed SST changes: Feedback effects associated with the simulation of cloud optical properties. *Clim. Dyn.* **5**: 175–187.

Liu H, Jacob D, Bey I, Yantosca R. 2001. Constraints from ^{210}Pb and ^{7}Be on wet deposition and transport in a global three-dimensional chemical tracer model driven by assimilated meteorological fields. *J. Geophys. Res.* **106**: 12109–12128, doi: 10.1029/2000JD900839.

Mahowald NM, Rasch PJ, Prinn GR. 1995. Cumulus parameterizations in chemical transport models. *J. Geophys. Res.* **100**: 26173–26189, doi: 10.1029/95JD02606.

Marley NA, Gaffney JS, Drayton PJ, Cunningham MM, Orlandini KA, Paode R. 2000. Measurement of ^{210}Pb, ^{210}Po, and ^{210}Bi in size-fractionated atmospheric aerosols: An estimate of fine-aerosol residence times. *Aerosol Sci. Technol.* **32**: 569–583.

Mircea M, Stefan S, Fuzzi S. 2000. Precipitation scavenging coefficient: Influence of measured aerosol and raindrop size distributions. *Atmos. Environ.* **34**: 5169–5174.

Preiss N, Genthon C. 1997. Use of a new database of lead 210 for global aerosol model validation. *J. Geophys. Res.* **102**: 25347, doi: 10.1029/97JD01389.

Pruppacher H, Klett J. 1996. *Microphysics of Clouds and Precipitation*, *Atmospheric and Oceanographic Sciences Library*. Springer: Berlin.

Radke LF, Hobbs PV, Eltgroth MW. 1980. Scavenging of aerosol particles by precipitation. *J. Appl. Meteorol.* **19**: 715–722.

Rasch PJ, Feichter J, Law K, Mahowald N, Penner J, Benkovitz C, Genthon C, Giannakopoulos C, Kasibhatla P, Koch D, Levy H, Maki T, Prather M, Roberts DL, Roelofs G-J, Stevenson D, Stockwell Z, Taguchi S, Kritz M, Chipperfield M, Baldocchi D, McMurry P, Barrie L, Balkanski Y, Chatfield R, Kjellstrom E, Lawrence M, Lee HN, Lelieveld J, Noone KJ, Seinfeld J, Stenchikov G, Schwartz S, Walcek C, Williamson D. 2000. A comparison of scavenging and deposition processes in global models: Results from the WCRP Cambridge workshop of 1995. *Tellus B* **52**: 1025–1056.

Reddy S, Boucher O. 2004. A study of the global cycle of carbonaceous aerosols in the LMDZT general circulation model. *J. Geophys. Res.* **109**, doi: 10.1029/2003JD004048.

Salzmann M, Lawrence MG, Phillips VTJ, Donner LJ. 2004. Modelling tracer transport by a cumulus ensemble: Lateral boundary conditions and large-scale ascent. *Atmos. Chem. Phys.* **4**: 1797–1811.

Schulze J, Auer M, Werzi R. 2000. Low level radioactivity measurement in support of the CTBTO. *Appl. Radiat. Isot.* **53**: 23–30.

Shapiro M, Forbes-Resha J. 1976. Mean residence time of ^{7}Be-bearing aerosols in the troposphere. *J. Geophys. Res.* **81**: 2647–2649, doi: 10.1029/JC081i015p02647.

Slinn WGN. 1983. Precipitation scavenging. In *Atmospheric Sciences and Power Production*, Chapter 11, Raderson D. (ed.). Division of Biomedical Environmental Research, US Department of Energy, Washington, DC.

Sportisse B. 2007. A review of parameterizations for modelling dry deposition and scavenging of radionuclides. *Atmos. Environ.* **41**: 2683–2698.

Tost H, Jöckel P, Lelieveld J. 2006. Influence of different convection parameterisations in a GCM. *Atmos. Chem. Phys. Discuss.* **6**: 9213–9257.

Tost H, Lawrence MG, Brühl C, Jöckel P, Team TG. 2010. Uncertainties in atmospheric chemistry modelling due to convection parameterisations and subsequent scavenging. *Atmos. Chem. Phys.* **10**: 1931–1951.

Winkler R, Dietl F, Frank G, Tschiersch J. 1998. Temporal variation of ^{7}Be and ^{210}Pb size distributions in ambient aerosol. *Atmos. Environ.* **32**: 983–991.

Yanai M, Chen B, Tung W-W. 2000. The Madden–Julian oscillation observed during the TOGA COARE IOP: Global view. *J. Atmos. Sci.* **57**: 2374–2396.

Yoshimori M. 2005. Beryllium 7 radionucleide as a tracer of vertical air mass transport in the troposphere. *Adv. Space Res.* **36**: 828–832.

